Sources of organic gases and aerosol particles and their roles in nighttime particle growth at a rural forested site in southwest Germany

Junwei Song[1,2], Harald Saathoff [1], Feng Jiang [1], Linyu Gao [1,2], Hengheng Zhang [1] and Thomas Leisner [1]

[1] Institute of Meteorology and Climate Research, Karlsruhe Institute of Technology, Hermann-von-Helmholtz-Platz 1, 76344 Eggenstein-Leopoldshafen, Germany

[2] Now at Univ. Lyon, Université Claude Bernard Lyon 1, CNRS, IRCELYON, 69626 Villeurbanne, France

Correspondence: Junwei Song (junwei.song@kit.edu) and Harald Saathoff (harald.saathoff@kit.edu)

Abstract

15   The composition, sources and chemical transformation of volatile organic compounds (VOCs) and organic aerosol (OA) particles were investigated during July-August 2021 at a rural forested site in southwest Germany 10 km north of the city of Karlsruhe. VOCs and semi-volatile OA particles were measured with a proton-transfer-reaction mass spectrometer coupled with a particle inlet (CHARON-PTR-MS). The CHARON-measured OA mass accounted on

20   average for 62 ± 18% of the total OA mass (4.2 ± 2.8 µg m^{-3}) concurrently measured by an aerosol mass spectrometer (AMS). The total concentrations of measured VOCs ranged from 7.6 to 88.9 ppb with an average of 31.2 ± 13.4 ppb. Positive matrix factorization (PMF) was used to identify major source factors of VOCs and OA. Three factors of oxygenated VOC (OVOC), namely aromatic-OVOCs, biogenic-OVOCs and aged-OVOCs contributed on

25   average 11% ± 9%, 37% ± 29%, 29% ± 21% of total VOC concentrations, respectively. The results of AMS-PMF indicated substantial contributions of oxygenated organic compounds to OA particle mass. Consistently, three secondary OA (SOA) factors determined by CHARON-PMF analysis, namely aromatic-SOA (5% ± 7%), daytime-biogenic SOA (17% ± 17%), nighttime-biogenic SOA (28% ± 21%), showed high contributions to total CHARON-measured

30   OA mass. Nighttime particle growth was observed regularly at this area, which was mainly attributed by the semi-volatile organic compounds and organic nitrates formed from the oxidation of monoterpenes and sesquiterpenes. This study presents major sources, real-time transformations of VOCs and OA, and nighttime particle formation characteristic for central European forested areas.

1 Introduction

Organic aerosol (OA) represents the majority of submicron aerosol mass (20-90%) in the atmosphere (Crippa et al., 2014; Zhang et al., 2011; Chen et al., 2022), which has adverse impacts on climate, air quality and human health (Ipcc, 2021; Burnett et al., 2014; Seinfeld and Pandis, 2016; Hallquist et al., 2009). OA particles can be either directly emitted from different sources (primary organic aerosol, POA) or formed by the oxidation of volatile organic compounds (VOCs) as secondary organic aerosol (SOA) (Shrivastava et al., 2017; Hallquist et al., 2009). Based on numerous field observations, SOA is often found to be the largest fraction of the submicron OA mass in different urban, rural and forest areas across Europe (44-100%) (Crippa et al., 2014; Chen et al., 2022), southeastern United States (47-79%) (Xu et al., 2015) and Asian countries (43-83%) (Zhou et al., 2020). However, the SOA concentrations are generally underestimated by current models, mainly due to incomplete understanding of sources and the transformation of VOCs to SOA (Jiang et al., 2019; Shen et al., 2019; Hodzic et al., 2016).

The Aerosol Mass Spectrometer (AMS) is widely used to quantify the OA mass at time resolutions of minutes (Decarlo et al., 2006). Mass spectral data from the AMS coupled with positive matrix factorization (PMF) allows for characterizing sources and evolution of OA (Ulbrich et al., 2009). AMS-PMF analysis is able to distinguish POA sources like traffic, cooking and biomass burning, and resolve factors for SOA such as semi-volatile oxygenated OA (SV-OOA) and low-volatility oxygenated OA (LV-OOA) based on their oxygenation degree and thus presumed volatility (Ng et al., 2010; Zhang et al., 2011; Crippa et al., 2014). The correlation of SV-OOA and LV-OOA with external tracers (e.g., ozone, temperature, relative humidity) can provide indirect evidence for their sources and formation mechanisms (Zhang et al., 2011). For instance, Canonaco et al. (2015) found that SV-OOA and LV-OOA positively correlated with ambient temperature in Switzerland in summer, which were attributed to the impacts of photochemistry and/or biogenic VOC (BVOC) emissions both enhanced by higher temperatures. In contrast, Crippa et al. (2014) reported a pattern for SV-OOA anticorrelated with temperature based on 25 AMS measurements across different European stations. Therefore, it remains difficulty to assign SOA factors (SV-OOA and LV-OOA) to specific sources or formation mechanisms by the AMS-PMF analysis without information on VOCs acting as SOA precursors. Proton transfer reaction-mass spectrometers (PTR-MS) are powerful instruments for detecting many VOC species especially SOA precursors like aromatic hydrocarbons, terpenoids, and oxygenated VOCs (OVOCs) (Jordan et al., 2009). The PMF analysis of VOC mass spectra from PTR-MS can constrain the sources of VOCs and resolve

secondary contributions of OVOCs (Wang et al., 2020a; Gkatzelis et al., 2021; Yuan et al., 2012). Furthermore, the CHemical Analysis of aeRosols ONline (CHARON) inlet coupled to the PTR-MS can detect the semi-volatile OA particles qualitatively and quantitatively (Eichler et al., 2015; Muller et al., 2017; Leglise et al., 2019). Compared to the AMS, the CHARON-PTR-MS subjects OA molecules with no significant thermal decomposition and less ionization-induced fragmentation (Gkatzelis et al., 2018a), thus it provides additional information on the detailed chemical composition of OA (Gkatzelis et al., 2018b; Muller et al., 2017). The concurrent measurements of AMS and CHARON-PTR-MS combined with PMF analysis can provide a comprehensive understanding in the sources of VOCs and the formation processes of SOA.

The chemical reactions of VOCs with atmospheric oxidants e.g., hydroxyl radicals (OH), ozone (O_3) and nitrate radicals (NO_3) can generate semi-volatile, low-volatile and extremely low volatile organic compounds (SVOC, LVOC and ELVOC) (Jimenez et al., 2009). These organic products are able to nucleate leading to new particle formation (NPF) and/or condense onto pre-existing particles contributing to particle growth and SOA mass (Ehn et al., 2014; Kirkby et al., 2016). In ambient observations, NPF has been mainly observed during daytime and was related to photochemical oxidation involving the formation of sulfuric acid and organic compounds (Kerminen et al., 2018). So far, only a few nighttime NPF events and/or particle growth events were observed in European rural and forest areas (Debevec et al., 2018; Huang et al., 2019; Kammer et al., 2018; Eerdekens et al., 2009), which are likely related to the oxidation of BVOCs. Kammer et al. (2018) observed high concentrations of monoterpenes and decreased O_3 during nighttime particle nucleation and growth stages in the Landes forest, France. Recently we found that highly functionalized organic nitrates generated from the reaction of NO_3 radicals with VOCs, can significantly contribute to the nighttime particle growth at a rural forested area in southwest Germany (Huang et al., 2019). However, the specific roles of oxidation of biogenic and anthropogenic VOCs to SOA formation and nighttime particle growth events are still not well understood also due to missing simultaneous measurements of VOCs and OA.

To follow our previous study (Huang et al., 2019), we performed online measurements of VOCs and OA particles by a CHARON-PTR-MS and an AMS during July-August 2021 at a rural forested area in southwest Germany. We present the composition of OA detected by the CHARON-PTR-MS in comparison to AMS measurements. The sources and evolution of OA and VOCs were investigated by the PMF analysis of VOCs and OA in combination with

meteorological conditions. In addition, we illustrate the roles of VOC oxidation and SOA formation for nighttime high OA mass and particle growth. Thereby, this study contributes to an improved understanding of evolution processes of VOCs and OA particles and characterizing nighttime particle growth occurring in summer in central European rural forested areas.

2 Methods

2.1 Measurement location

The campaign was carried out from July 17 to August 17, 2021 at a rural site in southwest Germany. As shown in Fig. 1, the measurement site (8.43ºE, 49.10ºN) is located on the rooftop of a temperature-controlled building (25 °C) on the campus north of the Karlsruhe Institute of Technology (hereafter KITcn) about 8 m above ground level. A canteen is located 300 m south of the sampling site in the campus, which is generally open for lunch time (11:30-14:00) at weekdays. Geographically, the campus is mostly surrounded by the Hardwald forest composed of mainly pine trees (e.g., Scots pine and European beech), which are important contributors for BVOC emissions. Besides, the measurement site is ~2-3 km east of the village Eggenstein-Leopoldshafen (pop. 15000), a mainly rural residential area, ~11 km north of downtown Karlsruhe (pop. 300000), ~8-10 km northeast of the Karlsruhe industrial areas including an 1815 MW coal-fired power plant and a refinery with 15.5Mt/yr capacity.

2.2 Instrumentation

An overview of all instruments used for this campaign is given in Table S1. Major instruments are described in the following.

2.2.1 CHARON-PTR-ToF-MS

A PTR-ToF-MS 4000X2 (Ionicon Analytik GmbH) coupled with a particle inlet (Chemical Analysis of aeRosol ONline, CHARON) was employed to measure the VOCs and semi-volatile aerosol particles. The details of conventional PTR-ToF-MS can be found elsewhere (Jordan et al., 2009). The PTR-ToF-MS 4000X2 used here is equipped with an ion funnel that reduces the ion loss and thus enhances the sensitivity (Pugliese et al., 2020). The CHARON inlet was described in detail elsewhere (Eichler et al., 2015; Muller et al., 2017). Briefly, the CHARON inlet consists of a charcoal denuder for stripping off gaseous organics, an aerodynamic lens for enriching particles in the instrument sub-sampling flow, and a thermo-desorption unit for particle evaporation prior to chemical analysis by the downstream PTR-ToF-MS. The particle enrichment factor of the CHARON inlet was calibrated with size-selected ammonium nitrate

particles (60-700 nm) at the beginning and end of the campaign. The average enrichment factor for 150-700 nm particles was 18.6 ± 2.4 (Fig. S1). A decreasing efficiency was found for smaller particles (< 150 nm).

In this campaign, the CHARON-PTR-MS was operated alternatingly measuring gas and particle phases programmed by the data acquisition software (IoniTOF 4.0, Ionicon Analytik GmbH). We set the program sequence with one full alternating measurement cycle lasting for 1 h including 5 min HEPA filter measurement for the particle background, 25 min for the CHARON particle phase measurement, 3 min transition to gas phase measurements, 25 min of VOC gas phase measurement and another 2 min transition. Generally, 2-3 min are sufficient for the re-equilibrium of instrumental conditions between different measurement modes (Piel et al., 2021). The PTR drift tube pressure, voltage and temperature were maintained constantly at 2.7 mbar, 450 V and 100 °C respectively, and the ion funnel was activated with a voltage of 45 V. These conditions result in a total E/N (E is the electric field, and N is the number density of the gas molecules in the drift tube) of ~120 Td for the VOC measurement. For the particle measurement, the thermo-desorption unit of CHARON inlet was set at a temperature of 150 °C and a pressure of 7-8 mbar, and the downstream PTR was automatically switched to 60 Td. In both gas and particle measurements, raw mass spectra including ions m/z from 15 to 398 Th were collected at a time resolution of 10 s. The mass resolution was ~2000-2800 $m/\Delta m$, where Δm is the full width at half mass for an ion peak of mass m.

During the gas-phase measurement, ambient air was sampled continuously from a 4.5 m long perfluoroalkoxy (PFA, 1/4'' OD) tube at a total flow of 8 L min^{-1}, and then a small subset of the flow (50-100 ml min^{-1}) was sampled by the PTR-ToF-MS through polyetheretherketone (PEEK) tubing maintained at 80 °C. Gas background were determined manually every two days by measuring synthetic air for 20-30 min. During the particle phase measurements, ambient particles were sampled by a PM$_{2.5}$ inlet (Comde-Derenda GmbH, 16.7 L min^{-1}) through a 3.45 m long stainless-steel tube and then a subset flow of ~550 ml min^{-1} was directed to the CHARON inlet. Particle background were determined automatically via the HEPA filter measurement. The residence time of ambient air was less than 1 s to minimize the loss of semi-volatile organic compounds.

Gas calibrations were performed at the beginning and end of the campaign, via dynamic dilution of a gas cylinder (Ionicon Analytik GmbH) containing 11 VOC species i.e., methanol, acetone, isoprene, benzene, toluene, $m/p/o$-xylenes, 1,3,5-trimethylbenzene, α-pinene and limonene (accuracy 10% at ~100 ppb). The sensitivity was in the range of ~1000 cps/ppb for

isoprene to 3000 cps/ppb for 1,3,5-trimethylbenzene. Raw data of the CHARON-PTR-MS were processed by the software Ionicon Data Analyzer (IDA 1.0.2, Ionicon Analytik) based on the algorithms by Müller et al., (2013). The details of CHARON-PTR-MS data analysis are given in Text S1 in the supplement.

2.2.2 HR-ToF-AMS

A High-Resolution Time-of-Flight AMS (Aerodyne Research Inc.) equipped with a $PM_{2.5}$ aerodynamic lens was used to measure the non-refractory $PM_{2.5}$ (NR-$PM_{2.5}$) components including OA, nitrate, sulfate, ammonium and chloride at a time resolution of 1 min (Decarlo et al., 2006; Williams et al., 2013). The operation of the AMS is explained in our previous publications (Song et al., 2022; Huang et al., 2019). Briefly, ambient air was sampled by a $PM_{2.5}$ inlet (flowrate 1 m^3 h^{-1}) shared with the CHARON through a 3.45 m long stainless-steel tube, and then a subset of the flow was sampled by the AMS at a flowrate of $\sim$84 cm^3 min^{-1}. The aerosol particles were then focused into a narrow beam by a $PM_{2.5}$ aerodynamic lens with an effective transmission for particle sizes ranging from $\sim$70 to $\sim$2500 nm (vacuum aerodynamic diameter, d_{va}) and heated by a vaporizer at 600 °C. The resulting vapors are ionized by electron impact (70 eV) and characterized by a time-of-flight mass spectrometer. The AMS ionization efficiency was calibrated by using ~400 nm dried ammonium nitrate aerosol particles. The AMS data was analyzed by the software package SQUIRREL 1.60C and PIKA 1.20C. To account for the effect of particle bouncing loss, chemical-composition-based collection efficiencies (~0.5) were applied to calculate the particle mass concentration (Middlebrook et al., 2012). Elemental analysis of OA including hydrogen-to-carbon ratio (H:C) and oxygen-to-carbon ratio (O:C) was calculated using the improved ambient method (Canagaratna et al., 2015).

2.2.3 Other instruments

The mass concentrations of $PM_{2.5}$ and PM_{10} were measured by an optical particle counter (OPC, Fidas200, Palas). The mass concentration of black carbon (BC) was measured by an aethalometer (AE33, Magee Scientific) with a time resolution of 5 min. The particle number concentrations (>2.5 nm) were measured by a water-based condensation particle counter (CPC3789, TSI Inc.). The particle number size distributions were measured by a nanoparticle sizer (NanoScan, TSI Inc.) ranging from 10-410 nm at a time resolution of 1 min and a scanning mobility particle sizer (SMPS, TSI Inc.) ranging from 13.6-763.5 nm at a time resolution of 7 min. A chemical ionization mass spectrometer utilizing iodide as reagent ion coupled with a Filter Inlet for Gases and AEROsols (FIGAERO-CIMS, Aerodyne Research Inc.) was deployed

200   for measuring oxygenated organic molecules in both gas and particle phases from 27th July to 9th August (Huang et al., 2019).

    The mixing ratios of ammonia (NH_3) were measured by cavity ring-down spectroscopy (G2103, Picarro Inc.). The concentrations of O_3 and NO_2 were measured by the gas monitors $O_3$41M and AS32M (both Environment S.A.). Due to data acquisition malfunction of gas

205   monitors, we adopted the hourly gaseous data of O_3, NO_2, NO and SO_2 obtained from the air quality monitor station Eggenstein (LUBW), located about 2.5 km southwest of the measurement site (Text S2, Figs. S2-S3). Meteorological data including temperature, relative humidity, wind direction and speed, global radiation and precipitation were measured on the rooftop by a compact sensor (WS700, Lufft). Planetary boundary layer (PBL) height data was

210   extracted from the European Centre for Medium-Range Weather Forecasts ERA5 reanalysis hourly data (Hersbach et al., 2020).

2.3 PMF receptor model

    The PMF analysis is widely used to identify the sources of VOCs (Gkatzelis et al., 2021; Wang et al., 2021; Wang et al., 2020a; Li et al., 2022; Pallavi et al., 2019; Yuan et al., 2012)

215   and OA (Crippa et al., 2014; Chen et al., 2022; Zhang et al., 2011; Xu et al., 2015; Song et al., 2022). The details of the PMF model can be found elsewhere (Paatero and Tapper, 1994). In this study, PMF analysis were performed on the VOC and OA datasets individually measured by the CHARON-PTR-MS and AMS using the Igor Pro-based PMF evaluation tool (PET v3.0).

    For the preparation of PMF analysis, low-molecular weight VOC species like formaldehyde

220   and methanol were excluded because they can come from many sources and cannot provide additional source information. In addition, less abundant VOC species with many missing data (≥20%) were also excluded for the input of PMF analysis. Finally, the dataset including 98 major VOC ions was used for the PMF analysis (Table S2). The average fraction of the 98 VOC ions to the total VOC signals was 85% ± 3% during the entire measurement period. Note that

225   PTR-ToF-MS cannot well detect some VOCs such as small alkanes and alkenes with a proton affinity lower than H_2O and/or highly oxidized organic species. However, the PMF analysis of VOC data measured by the PTR-ToF-MS still has advantages in understanding the biogenic and anthropogenic emission sources and their potential contributions to secondary VOC and particle formation (Wang et al., 2020a; Gkatzelis et al., 2021; Li et al., 2022; Wu et al., 2022).

230   In this study, the uncertainty matrix data were determined according to the method detection limit (MDL) of each VOC ion and the error fraction (Paatero et al., 2014).

Based on the high-resolution mass spectra of AMS-measured OA (m/z 12-120), an unconstrained PMF analysis was performed to resolve the sources of OA (Ulbrich et al., 2009). Note that no constrained PMF analysis of AMS-measured OA was performed in this study as it cannot improve the interpretation of SOA factors. In addition, we performed a PMF analysis of CHARON-measured OA mass spectra (m/z 60-300) with chemical formula assigned organic molecules. We excluded some small particulate ions like $C_3H_5^+$ and $C_3H_7^+$ for the PMF analysis because they could be contributed by the fragmentation of multiple organic compounds and cannot provide useful source information.

2.4 Air mass back-trajectory analysis

To investigate the impact of air mass origins on atmospheric pollutants, seventy-two-hour back-trajectories with an altitude of 100 m were computed for every hour by using the National Oceanic and Atmospheric Administration (NOAA) Air Resources Laboratory Hybird Single-Particle Lagrangian Integrated Trajectory (HYSPLIT) model (Stein et al., 2015). Then all trajectories were grouped into different clusters based on their similarity in spatial distribution (Petit et al., 2017).

3 Results and discussion

We first give an overview of our measurements and then discuss the different sources assigned according to the PTR-MS-measured VOCs, AMS-measured OA particles and CHARON-measured semi-volatile OA particles. Then we will discuss the role of air mass origins on sources of VOCs and OA particles. Finally, we will discuss the contribution of semi-volatile organic compounds to nighttime particle formation and growth.

3.1 Overview of the field observations

The time series of meteorological parameters during the entire campaign is given in Fig. 2. The ambient temperature and relative humidity ranged from 10.8 to 32.2 ºC (average: 20.2 ± 4.3 ºC) and 32% to 99% (71% ± 17%) respectively. The wind speeds varied from <0.1 to 3.9 m s^{-1} (0.97 ± 0.6 m s^{-1}). The measurement site was subject to urban and industrial emissions especially for southwesterly wind directions (Fig. 1). With HYSPLIT analysis, 783 air mass backward trajectories in total were obtained for the entire campaign, which were grouped into five clusters. Cluster 1 (C1) shows the southwesterly air masses passing through France and the urban area of Kalsruhe (29% fraction), while C2 reflects air masses from northern Germany (10% fraction) also transported over forested areas, and C3 (16% fraction) are the air masses

originating from the North Sea and also passing through forested areas. In addition, C4 (31%) and C5 (14%) are air masses transported from the Atlantic Ocean.

265   The total mixing ratios of measured VOCs (98 VOC ions) ranged from 7.6 to 88.9 ppb with an average of 31.2 ± 13.4 ppb. As shown in Fig. S4, the average mixing ratios of isoprene, monoterpenes and sesquiterpenes were 1.61 ± 0.96 ppb, 1.71 ± 2.48 ppb and 6.5 ± 14.8 ppt, respectively. The diurnal variation of isoprene showed a clear increase during daytime, which was related to the emissions of isoprene enhanced by temperature and sunlight (Fig. S5). In

270 contrast, monoterpenes and sesquiterpenes showed higher concentrations at night and very low levels during daytime. Generally, higher temperatures lead to increased emissions of monoterpenes and sesquiterpenes, while their concentrations can be rapidly depleted by photochemical oxidation as well as increased PBL height during daytime (Hellén et al., 2018). Compared to isoprene and monoterpenes, lower concentrations of benzene (0.30 ± 0.23 ppb)

275 and toluene (0.28 ± 0.22 ppb) were observed.

     The average mass concentration of $PM_{2.5}$ measured by the OPC was 6.0 ± 3.6 µg m^{-3} over the entire campaign (Fig. 2c). The time series of mass concentrations of NR-$PM_{2.5}$ measured by the AMS plus BC agrees well with the OPC-measured $PM_{2.5}$ (Fig. S6). OA was the largest contributor with average contributions of $67\% \pm 11\%$ to the total $PM_{2.5}$ mass, followed by

280 sulfate ($23\% \pm 9\%$), BC ($7\% \pm 3\%$), ammonium ($6\% \pm 2\%$), nitrate ($3\% \pm 2\%$) and chloride (<1%). The average OA mass (4.2 ± 2.8 µg m^{-3}) was within the range (0.9-8.2 µg m^{-3}) observed at other European rural sites (Crippa et al., 2014). However, the OA mass was slightly lower than that (5.0 ± 3.3 µg m^{-3}) reported by our previous study conducted at Linkenheim in summer 2016, ~2 km northwest of the measurement site (Huang et al., 2019). This could be caused by

285 wet scavenging by frequent rainfall in present study (Fig. 2b). During the campaign, the particle number size distributions showed regular particle growth starting after sunset and lasting well into the morning of the following day. Similar nighttime particle growth has been observed at near our measurement location during previous summers (Huang et al., 2019). More discussions of nighttime particle growth are presented in Section 3.4.

290   The time series of OA measured by the CHARON with ion mass range of m/z 60-300 showed a good agreement with that of AMS-measured OA (r = 0.93). On average, the CHARON can detect $62\% \pm 18\%$ of total OA mass measured by the AMS, which is comparable to the mass recovery of biogenic SOA measured by the CHARON-PTR-MS to SMPS mass ($80\% \pm 10\%$) in chamber experiments (Gkatzelis et al., 2018a). Figure S7 shows the median

295 OA mass spectra of CHARON-PTR-MS measurements averaged over the entire campaign.

Mass concentrations associated with individual m/z signal ranged from 0.2 ng m^{-3} to 183 ng m^{-3}. A total of 191 species are well assigned (Fig. 3 and Table S3), contributing to 72% $\pm$ 5% of total CHARON-measured OA mass. The majority of ions detected by the CHARON are present in the lower mass range ($m/z<250$), which is mainly due to the fragmentation of larger masses during the ionization processes of PTR-MS (Muller et al., 2017; Gkatzelis et al., 2018a). Figure 3a shows the mass distributions associated with pure and oxygenated hydrocarbon ions ($C_xH_y^+$ and $C_xH_yO_z^+$), resolved by carbon and oxygen atom numbers. The most abundant species are characterized with by a formula of $C_xH_yO_2^+$, accounting for 30% $\pm$ 4% of total OA measured by the CHARON, followed by $C_xH_y^+$ (13% $\pm$ 3%), $C_xH_yO_1^+$ (11% $\pm$ 3%) and $C_xH_yO_3^+$ (10% $\pm$ 2%). It is consistent with previous studies that CHARON-PTR-MS is suitable to measure the semi-volatile and less-oxidized organic compounds ($C_xH_yO_{1-3}^+$) in the particle phase. However, the detection of highly oxidized organic species is limited due to the thermo-desorption temperature of CHARON (150 ºC) and the fragmentation during PTR ionization. Figure 3 shows the diurnal variations of $C_xH_yO_{0-5}^+$ during the entire measurement period. The groups of $C_xH_yO_{0-2}^+$ showed higher concentrations during nighttime. Previous studies have reported that $C_xH_y^+$ can be attributed to hydrocarbon-like compounds or the fragmented ions of oxygenated ions through the neutral loss of water (-H_2O), a carbonyl group (-CO) and a carboxyl group (-CO_2) (Gkatzelis et al., 2018b; Peng et al., 2023). The time series of $C_xH_y^+$ strongly correlated with $C_xH_yO_1^+$ (r = 0.98) and $C_xH_yO_2^+$ (r = 0.82), suggesting that they were mainly contributed by the fragmentation of oxygenated ions at higher masses. In contrast, $C_xH_yO_{3-5}^+$ showed peak concentrations at noon, suggesting that they were related to daytime photooxidation processes.

3.2 Source identification of organic aerosol compounds

3.2.1 Source attribution of VOCs (PTR-MS)

In this study, a five-factor solution was selected as the optimum and interpretable solution for the PMF analysis of VOCs. After carefully checking the factor profiles, diurnal patterns, and correlations with external tracers (Fig. 4 and Fig. S8), we assigned these five VOC factors as traffic VOCs, terpenes, OVOCs related to aromatic hydrocarbon oxidation (aromatic-OVOCs), OVOCs related to BVOC oxidation (biogenic-OVOCs,) and OVOCs related to aged air masses (aged-OVOCs). They constituted 12% $\pm$ 13%, 11% $\pm$ 16%, 11% $\pm$ 9%, 37% $\pm$ 29% and 29 $\pm$ 21% of total VOC mixing ratios on average during the entire campaign, respectively.

The first factor was identified as traffic VOC emissions with high contributions to aromatic hydrocarbon ions such as $C_6H_7^+$ (m/z79.05), $C_7H_9^+$ (m/z93.07), $C_8H_9^+$ (m/z105.07), $C_8H_{11}^+$ (m/z107.09), $C_9H_{13}^+$ (m/z121.10) and $C_{10}H_{15}^+$ (m/z 135.12). They can be assigned to benzene,

toluene, styrene, xylenes, C_9-aromatics and C_{10}-aromatics correspondingly, which are typical
tracers for vehicular emissions (Gkatzelis et al., 2021; Wang et al., 2021; Crippa et al., 2013b).
This factor also had the predominant contribution to $C_2H_7O^+$ (m/z47.05, ethanol), which was
mainly attributed to the emissions of ethanol-gasoline fueled cars in the campus. Good
correlations were found for the traffic VOC factor with ethanol (r = 0.82), benzene (r = 0.67)
and toluene (r = 0.82). The diurnal variation of this factor peaked the morning rush hours (7:00-
9:00), supporting that it was related to traffic emissions. A shown in Fig. S9, the bivariate polar
plot analysis showed that higher concentrations of traffic VOC factor were observed at the wind
sector of northeast with low wind speeds (0-1.5 m s^{-1}), suggesting that it was related to local
traffic emissions.

The second VOC factor was characterized as terpenes with dominant contributions to $C_5H_7^+$
(m/z67.50), $C_6H_9^+$ (m/z81.70), $C_7H_{11}^+$ (m/z95.80), $C_{10}H_{17}^+$ (m/z137.13), $C_{11}H_{17}^+$ (m/z149.10)
and $C_{15}H_{25}^+$ (m/z205.20). $C_{10}H_{17}^+$ and $C_{15}H_{25}^+$ were assigned as monoterpenes and
sesquiterpenes respectively, while $C_5H_7^+$, $C_6H_9^+$, $C_7H_9^+$ and $C_{11}H_{17}^+$ are fragment ions from
monoterpenes and sesquiterpenes formed inside the PTR instrument (Kari et al., 2018; Tani et
al., 2003; Kim et al., 2009). The O/C ratio of terpene factor was low (0.07). As expected, the
time series of the terpene factor correlated tightly with that of monoterpenes (r = 0.99) and
sesquiterpenes (r = 0.88). The diurnal cycle of the terpene factor showed higher concentrations
during nighttime. However, a fast decrease of terpenes was observed during daytime, which is
due to rapid consumption of monoterpenes and sesquiterpenes by photochemical oxidation and
furthermore by the increasing PBL heights.

The third VOC factor contains abundant oxygenated aromatic hydrocarbon ions such as
$C_7H_8O_{1-3}H^+$, $C_8H_{10}O_{2-3}H^+$, $C_9H_{10}O_{1-3}H^+$ and $C_9H_{12}O_{1-3}H^+$, which are attributed to gaseous
products of aromatic hydrocarbon oxidation. For example, $C_7H_8O_1H^+$, $C_7H_8O_2H^+$ and
$C_7H_8O_3H^+$ can be assigned as cresol, dihydroxy-toluene and dicarbonyl-epoxide, which have
been identified as products from toluene oxidation in simulation chamber studies (Zaytsev et
al., 2019). Wang et al. (2020b) identified $C_9H_{10}O_{1-3}H^+$ and $C_9H_{12}O_{1-3}H^+$ as gaseous products of
trimethylbenzene oxidation in laboratory experiments. The time series of the third VOC factor
correlated well with those of gaseous products of aromatic oxidation e.g., $C_7H_8O_{1-3}H^+$ (r = 0.78-
0.85) and $C_9H_{10}O_{1-3}H^+$ (r = 0.88-0.92). Therefore, we defined it as an oxygenated VOC factor
related to aromatic hydrocarbon oxidation (aromatic-OVOCs). The diurnal cycle of aromatic-
OVOCs showed a peak at morning rush hours (7:00-9:00), which was likely related to the
oxidation of aromatic hydrocarbons from traffic emissions. We also observed a weaker peak of

aromatic-OVOCs during afternoon rush hours (16:00-17:00). This can be explained by a stronger dilution in the expanded PBL for the afternoon rush hour.

The fourth VOC factor was characterized by high contributions to smaller oxygenated VOC (OVOC) such as $CH_2O_2H^+$, $C_3H_4OH^+$, $C_2H_4O_2H^+$ and $C_3H_6O_2H^+$, which can be assigned as formic acid, acrolein, acetic acid, and propionic acid, correspondingly. In addition, $C_4H_6OH^+$ is an important constituent in this factor, which was attributed to the isoprene oxidation products as methyl vinyl ketone and/or methacrolein (MVK+MACR) (Wennberg et al., 2018). The O/C ratios of this factor (0.39) was higher than that of terpene factor (0.07). The time series of this factor showed strong correlations with that of formic acid (r = 0.96), acetic acid (r = 0.95), MVK + MACR (r = 0.81) as well as O_x ($NO_2 + O_3$, r = 0.86), an indicator of photochemical oxidation processes. It suggests that this VOC factor was mainly related to the photochemical oxidation processes of BVOCs. The diurnal variations of this factor showed significantly higher concentrations during daytime. Moreover, the bivariate polar plot analysis showed that high concentrations of this factor were observed at the wind sectors of east and southeast, suggesting that it was mainly related to the biogenic emissions. Therefore, this VOC factor can be attributed to OVOCs related to BVOC oxidation (biogenic-OVOCs). Recently, Li et al., (2021) reported that the daytime oxidation of monoterpenes could produce more-oxidized gaseous organic compounds (e.g., $C_{10}H_{15}O_{4-6}H^+$ and $C_{10}H_{16}O_{4-6}H^+$) in the French Landes forest according to the binned PMF analysis of VOCs detected by a Vocus-PTR-MS. In the present study, these more-oxidized monoterpene-derived gaseous organic compounds in the gas phase cannot be well detected by our PTR-MS, and thus are not included for further PMF analysis.

The fifth VOC factor consists of lower molecular weight OVOCs such as $C_3H_4O_2H^+$, $C_2H_4O_3H^+$, $C_3H_4O_3H^+$, $C_5H_2O_2H^+$, $C_4H_2O_3H^+$, and $C_6H_4O_2H^+$. This VOC factor had no specific marker ions related to sources and/or formation processes. Its time series exhibited insignificant temporal variation compared to other VOC factors, but showed a similar trend as the variation of wind direction (r = 0.53). The diurnal variations of this factor were less pronounced during the entire campaign. The O/C ratio of this factor (r = 0.39) was higher than that of other VOC factors like terpenes and traffic VOC (0.07-0.31). The bivariate polar plot analysis showed that high concentrations of this factor were observed at west or southwest wind sectors with high wind speeds. Consistently, the long-range transported Atlantic air mass clusters (C4 and C5) had high fractions of this factor to total VOC mixing ratios. Based on these results, the fifth VOC factor can be denoted as the OVOCs associated with the advection of aged air masses (aged-OVOCs).

3.2.2 Source apportionment of OA particles (AMS)

A five-factor solution was selected as the optimal results of PMF analysis of AMS-measured OA (Fig. 5 and Fig. S10) These five factors were denoted as a hydrocarbon-like OA (HOA), two semi-volatile oxygenated OA (SV-OOA1 and SV-OOA2), a low-volatile oxygenated OA (LV-OOA) and a marine-related oxygenated OA (MOOA). They constituted 6% ± 5%, 20% ± 12%, 17% ± 9%, 35% ± 17% and 22% ± 16% of total OA mass on average during the entire campaign.

The first OA factor was HOA dominated by alkyl fragments such as $C_3H_5^+$, $C_3H_7^+$, $C_4H_7^+$ and $C_4H_9^+$, which was similar to that from traffic emissions reported in previous studies (Canagaratna et al., 2004; Crippa et al., 2014). The time series of HOA correlated well with the traffic VOC factor (r = 0.72) and moderately with BC (r = 0.52), confirming that they are related to primary traffic emissions. The correlation of HOA and BC could be deteriorated due to the different emission ratios of HOA/BC of different vehicles and fuel types of the cars passing the sampling site. Generally, gasoline vehicles have higher emission ratios of HOA/BC (0.9-1.7) than diesel vehicles (0.03-0.61) (Dewitt et al., 2015). In this study, the average HOA/BC was 0.38 ± 0.31, suggesting the dominant contributions of diesel vehicles. The diurnal cycle of HOA showed a peak at the morning rush hours (8:00-9:00). No HOA peak was found in the afternoon, which is likely associated with that strong photochemical oxidation, high wind speeds and expanded PBL in the afternoon leading to the decrease of HOA mass. In addition, the bivariate polar plot analysis also showed that HOA was associated with the northeast sector with low wind speeds (0-1.5 m s^{-1}), suggesting that HOA was mainly attributed to local traffic emissions.

The second and third OA factors were two semi-volatile oxygenated OA (SV-OOA) factors with different mass spectra and temporal variations. The O:C ratios of SV-OOA1 and SV-OOA2 were 0.45 and 0.51 respectively, which are within the typical range of 0.2-0.6 reported for SV-OOA identified from many AMS measurements (Ng et al., 2010). Good correlation was found between SV-OOA1 and particulate nitrate (r = 0.73), indicating their semi-volatile nature. Besides, SV-OOA1 showed a good correlation with the VOC terpene factor (r = 0.71). SV-OOA1 showed distinct diurnal patterns with higher mass concentrations during nighttime. Therefore, SV-OOA1 was related to the nighttime oxidation of terpenes. In contrast, SV-OOA2 had less pronounced diurnal variation. SV-OOA2 showed a good correlation with aromatic-OVOC factor (r = 0.70). Furthermore, we observed that the mass concentrations of SV-OOA2 increased from 10-14th August when the air masses were transported from urban Karlsruhe. Therefore, SV-OOA2 was likely related to urban emissions. Please note that we cannot attribute

SV-OOA1 and SV-OOA2 to specific anthropogenic and biogenic sources solely based on the AMS-PMF analysis.

430   The fourth OA factor was identified as low-volatile oxygenated OA (LV-OOA) with higher O:C ratios of 0.86. The mass spectrum of LV-OOA was distinguished by the predominant ions of m/z44 (CO_2^+) and m/z28 (CO^+), which is consistent with previous observations for LV-OOA from AMS measurements (Ng et al., 2010). LV-OOA showed a good correlation with CO_2^+ (R = 0.96), fair correlations with O_x (r = 0.48) and the biogenic-OVOC factor (r = 0.58). This

435   indicates that LV-OOA was mainly contributed by the photochemical oxidation of BVOCs. As expected, the diurnal cycle of LV-OOA showed a peak at the afternoon (12:00-14:00) with higher temperatures and O_3 levels as well as intensive radiation. The bivariate polar plot analysis showed that high concentrations of LV-OOA were observed at the wind sectors of east and/or southeast, suggesting that it was mainly associated with the oxidation of biogenic

440   emissions.

        The fifth OA factor was denoted as a marine oxygenated OA (MOOA) with the highest O/C ratio of 1.00. The time series of MOOA strongly correlated with m/z 79 ($CH_3SO_2^+$, r = 0.84), an ion derived from the fragmentation of methanesulfonic acid (MSA) as a marker of marine sources (Crippa et al., 2013a; Huang et al., 2018). Base on the back-trajectory analysis, the

445   concentrations of MOOA showed significantly increase at dry days when the measurement site was influenced by the air masses from the Atlantic Ocean. Crippa et al. (2013a) identified a MOOA factor in Paris, France in summer 2009, where a significant increase of MOOA mass was also observed for air masses from the Atlantic Ocean. In this study, MOOA showed a higher O:C ratio compared to that (0.57) observed in Paris in summer 2009 (Crippa et al.,

450   2013a). Furthermore, the diurnal variation of MOOA was relatively flat during the entire measurement period. The bivariate polar plot analysis also showed that high concentrations of MOOA were observed at the wind sectors of west with high wind speeds. The results confirm that MOOA was associated with aged marine emissions from the Atlantic Ocean. This is in line with the finding by (Shen et al., 2019) that the aerosol particles in this region are influenced by

455   marine emission from the Atlantic Ocean in summer.

3.2.3 Source attribution of semi-volatile OA particles (CHARON)

        In this study, a six-factor solution (Fig. 6 and Fig. S11) was selected as the best interpretable solution for the PMF analysis of OA measured by the CHARON-PTR-MS including two factors that couldn't be assigned to a specific source (F5 and F6). The four factors assigned can be

460   defined as cooking-related OA (COA), SOA related from aromatic oxidation (aromatic-SOA),

and SOA related to daytime and nighttime BVOC oxidation, respectively (daytime- and nighttime-BSOA, cf. Fig. 6). They contributed to 9% ± 9%, 5% ± 5%, 17% ± 17% and 28% ± 21% of total OA mass measured by the CHARON, and the unassigned factors (F5 and F6) accounted for 16% ± 18% and 26% ± 23%, respectively during the entire campaign.

465 The first OA factor was characterized with high fraction of $C_7H_9^+$, $C_{16}H_{33}O_2^+$ and $C_{16}H_{35}O_3^+$. $C_{16}H_{33}O_2^+$ and $C_{16}H_{35}O_3^+$ can be tentatively assigned as long-chain fatty acids. For example, $C_{16}H_{33}O_2^+$ was tentatively assigned as palmitic acid, which is a fatty acid mainly released from the cooking emissions. Palmitic acid can be used as a tracer for cooking-related OA (Reyes-Villegas et al., 2018). Furthermore, the diurnal variation of this factor showed a

470 peak at lunch time (12:00-14:00), which is in line with the opening hours of the canteen located 300 m south of the sampling site in the campus. Therefore, it is reasonable to assign this factor associated with cooking emissions. As expected, the time series of COA well correlated with $C_{16}H_{33}O_2^+$. Note that we cannot assign particulate $C_7H_9^+$ ion to specific organic compounds, which is likely produced from the fragmentation of oxidized organic compounds at higher mass.

475 In this study, the COA factor was not resolved from the unconstrained AMS-PMF analysis, which is likely due to the lack of specific marker ions of cooking emissions measured by the AMS. On other hand, cooking-related oxidized species may be mixed into HOA resolved from the AMS-PMF analysis, which leads to HOA having a high O:C value (0.26) A (Mohr et al., 2012).

480 The second OA factor was defined as aromatic-SOA characterized with high fractions of $C_{6-9}H_yO_{1-3}^+$, which are likely oxidation products of aromatic hydrocarbons as indicated by previous chamber studies (Wang et al., 2020b; Zaytsev et al., 2019). The time series of this factor correlated with oxygenated aromatic hydrocarbon ions e.g., $C_7H_9O_3^+$ (r = 0.86). Furthermore, we observed an enhancement of aromatic-SOA during 10th-14th August with the

485 influence of urban air masses (Fig. 6). Despite the dilution of the boundary layer during the day, there is little variation in the aromatic-SOA concentration during the day. The transport of aromatic-SOA from urban Karlsruhe might offset the dilution effects of the expanding boundary layer. The time series of aromatic-SOA showed a good correlation (r = 0.82) with SV-OOA2 from the AMS-PMF analysis (Fig. 7), indicating that SV-OOA2 can be attributed to

490 the oxidation of aromatic hydrocarbons.

 The third OA factor contains high contributions from ions such as $C_{10}H_{15}O^+$, $C_{10}H_{17}O^+$ and $C_{10}H_{13}O_{2-3}^+$, which can be identified as weakly oxidized products of monoterpenes or their fragments (Li et al., 2021; Gkatzelis et al., 2018b). As expected, the time series of this factor

correlated tightly with $C_{10}H_{17}O^+$ (r = 0.91). This factor showed distinct diurnal pattern with high concentrations during nighttime, suggesting that it was associated with the nighttime chemistry and thus defined the as a nighttime-BSOA. Besides, the time series of nighttime-BSOA correlated well with SV-OOA1 from the AMS-PMF analysis (r = 0.63, Fig. 7). This confirms that SV-OOA1 was mainly attributed to the less-oxidized organic compounds formed from the nighttime oxidation of terpenes.

The fourth OA factor shows high contributions from ions such as $C_8H_{13}O_{3-5}^+$, $C_9H_{13}O_{3-4}^+$, $C_{10}H_{13}O_{4-5}^+$ and $C_{10}H_{15}O_{4-5}^+$. These ions can be related to more oxidized products of monoterpene oxidation and/or their fragments as reported in previous chamber studies and field observations (Li et al., 2021; Gkatzelis et al., 2018b). The diurnal variation of this factor showed increased concentrations during daytime. These results suggest that this factor is associated with SOA formed from the oxidation of biogenic VOCs during daytime and thus denoted as a daytime-BSOA. The time series of daytime-BSOA showed a weak correlation with LV-OOA from the AMS-PMF analysis (r = 0.40). Note that the CHARON-PTR-MS cannot well measure low-volatility organic compounds, which may deteriorate the correlation between daytime-BSOA and LV-OOA to some extent.

In addition, two other factors (F5 and F6) were resolved from the PMF analysis of CHARON-measured OA. The mass spectra of both F5 and F6 dominated by the ion $C_3H_5O_2^+$. Figure S12 shows the time evolution of particulate $C_3H_5O_2^+$ at an individual CHARON-PTR-MS alternatingly measurement cycle. It can be seen that CHARON showed slow response to particulate $C_3H_5O_2^+$ compared to other low-molecular weight ions such as ($C_4H_7O^+$ and $C_4H_9O^+$). This suggests that particulate $C_3H_5O_2^+$ can be associated with less-volatile organic compounds. Note that $C_3H_5O_2^+$ is attributed to the fragmentation of multiple species, which cannot be regarded as a source marker ion. We found that the time series of F6 correlated better with MOOA resolved from the AMS-PMF analysis (r = 0.4) compared to that of F5 (r = 0.1). The time series of F5+F6 showed a better correlation with MOOA (r = 0.59, Fig. S14). The results suggest that F6 was likely related to the long-range transported Atlantic air masses. Due to the lack of source marker compounds, we currently cannot assign these two factors to specific sources or formation processes explicitly in this study.

3.3 Impact of air mass origin on VOC and OA sources

Figure 8 shows the relative contributions of VOC factors to total VOC mixing ratios and OA factors to total OA mass measured by the AMS for five different air mass clusters. Both continental air mass clusters C1 and C2 showed highest fractions of biogenic-OVOCs to total

VOC mixing ratios (40% and 55%), indicating the importance of biogenic VOC oxidation to OVOC contribution. Comparatively, lower fraction of biogenic-OVOCs (30% and 35%) were observed for long-range transported air masses from Atlantic Ocean (C4-C5). Furthermore, C4

530 and C5 had high fractions of aged-OVOCs in total VOC mixing ratios, suggesting the importance of long-range transport of air masses for the variations of VOCs. Compared to other air mass clusters, we found highest fractions of aromatic-OVOCs in C1, which reflects increased anthropogenic emissions from the downtown Karlsruhe. Besides, high fractions of traffic VOCs were observed for C2 and C3, which was mainly related to local traffic emissions.

535 All air mass clusters showed high fractions of LV-OOA in total OA mass (24%-52%), indicating the importance of photochemical oxidation of biogenic VOCs to SOA formation. High fractions of MOOA in total OA mass were observed for the Atlantic air masses (C4 and C5). Please note that MOOA played an important role for relatively clean periods with low OA mass. Interestingly, high fractions of SV-OOA2 in total OA mass were observed for C1, C4

540 and C5 (17%-21%) with the air masses having passed over the urban Karlsruhe compared to those for C2 and C3 (10%-11%) which passed over forested areas. However, the fractions of SV-OOA1 in total OA mass showed no significant changes among different air mass clusters. In total, high fractions of SOA factors including SV-OOA1, SV-OOA2 and LV-OOA were found from 63% for C5 to 87% for C2, emphasizing the important secondary aerosol

545 contributions over the primary HOA and long-range transported MOOA.

Overall, we conclude that local BVOC oxidation can produce low-molecular weight biogenic-OVOCs and LV-OOA during daytime while leading to the formation of SV-OOA1 during nighttime. In contrast, the air masses transported from urban Karlsruhe can increase the role of aromatic OVOCs and SV-OOA2 in the variations of VOCs and OA.

550 **3.4 Contribution of semi-volatile organic compounds to nighttime particle growth**

Figure 9 shows the diurnal variations of geometric mean particle diameters, traffic VOC and terpene factors, atmospheric oxidants, mass concentrations and fractions of OA, SV-OOA1 and SV-OOA2 during the periods influenced by five different air mass clusters. The geometric mean particle diameter showed evidently increases during nighttime (20:00-06:00 next day)

555 especially for the air mass clusters of C1-C3. Simultaneously, the diurnal variations of OA mass also exhibited significantly increases during nighttime of air mass clusters C1-C3. Among the OA components, both SV-OOA1 and SV-OOA2 mass showed fast increases during nighttime, correspondingly. Note that the mass increase of OA, SV-OOA1 and SV-OOA2 could be related to nighttime chemistry and the shrinking of the boundary layer. No significant differences of

560   diurnal patterns of boundary layer height were found among different air mass clusters except for C5 with slightly high boundary layer height during nighttime (Fig. S15). Furthermore, we calculated the diurnal variations for the mass fractions of SV-OOA1 and SV-OOA2 in total OA mass to normalize the impact of meteorology. The mass fraction of SV-OOA1 showed still significant increases during nighttime from 10% to 40% for C1-C3 and 10% to 25% for C4-C5.

565   In contrast, the mass fraction of SV-OOA2 showed less pronounced diurnal variations for all air mass clusters. This indicates that the formation of SV-OOA1 dominated the nighttime particle growth and high OA mass rather than SV-OOA2. Furthermore, high concentrations of terpenes were observed along with the decrease of O_3 during nighttime supporting the formation of SV-OOA1. Although the traffic VOC factor mainly containing aromatic hydrocarbons also

570   showed higher concentrations during nighttime, these species have lower reactivity towards O_3 compared to terpenes (Atkinson, 2000). Therefore, we exclude the possibility of nighttime oxidation of aromatic hydrocarbons leading to the enhancement of SV-OOA1 formation.

    In addition to O_3, terpenes can react with nitrate radicals (NO_3) during nighttime, resulting in the formation of organic nitrate. In this study, we calculated the total organic nitrate from the

575   AMS measurement (Farmer et al., 2010; Kiendler-Scharr et al., 2016; Xu et al., 2015; see details in Text S3). We also calculated the production rate of NO_3 radicals (P_{NO_3} = k[NO_2][O_3], k = 3.5 x 10^{-17} cm^3 molecules^{-1} s^{-1} at 298 K, IUPAC) by using the measured concentrations of O_3 and NO_2 (Huang et al., 2019). The diurnal variations of P_{NO_3} showed significant increases after 20:00 in all air mass clusters especially for C2 and C3 with the forest air masses.

580   Simultaneously, the mass concentrations of organic nitrate showed rapid increases over the nighttime. Furthermore, the mass fraction of organic nitrate in OA showed significant increase during nighttime for all air mass clusters. Given the high concentrations of monoterpenes and sesquiterpenes during nighttime, we assume that the organic nitrate was mainly formed from the oxidation of biogenic VOCs by NO_3 radicals. Furthermore, we found that organic nitrate

585   showed better correlations with particulate organic nitrate molecules $C_{10}H_{15}O_7N$ (r = 0.46) and $C_{15}H_{23}O_7N$ (r = 0.55) compared to $C_5H_7O_7N$ (r = 0.22) measured by the FIGAERO-CIMS (Fig. S16). According to chamber studies and field observations, $C_5H_7O_7N$, $C_{10}H_{15}O_7N$ and $C_{15}H_{23}O_7N$ can be attributed to organic nitrate products formed from isoprene, monoterpenes and sesquiterpenes, respectively (Huang et al., 2019; Chen et al., 2020; Faxon et al., 2018; Wu

590   et al., 2021; Gao et al., 2022). Based on above results, we can conclude that organic nitrate was mainly contributed by the NO_3 radical-induced oxidation of monoterpenes and sesquiterpenes. The concentrations of steady state NO_3 radicals were also roughly estimated in supplement Text

595   Finally, we present two cases showing the nighttime particle growth with increased OA mass (Fig. 10). Please note that this is actually a phenomenon observed regularly in this area in summer (Huang et al., 2019). The first case (Case 1) was from 21st-23rd July 2021 with the influence of forest air masses, while the second one (Case 2) was from 28th-30th July 2021 with impact of long-range transported Atlantic air masses. It can be clearly seen that the particle

600 growth during nighttime started from 20:00 local time with linear increases of geometric mean particle sizes reaching maximum values at 04:00-06:00 next day in both cases. We calculated the particle growth rate by averaging the geometric mean particle diameter difference from 20:00 to 04:00 on the next day. The particle growth rates for two nights of Case 1 were 3.9 and 4.0 nm hr^{-1} respectively, which were close to those (5.3 ± 3.1 nm hr^{-1}) observed at the same area

605 in summer 2016 and 2018 (Huang et al., 2019) and lower than the nighttime growth rates observed at Landes forest (9.0-15.7 nm hr^{-1}) (Kammer et al., 2018). About a factor of two lower particle growth rates were found for two nights of Case 2 with 1.8 and 1.5 nm hr^{-1}, respectively. In the same way, we calculated the mass increase rate of SV-OOA1 and organic nitrate by averaging the mass difference correspondingly. Consequently, the mass increase rates of SV-

610 OOA1 were 0.36 and 0.53 µg m^{-3} hr^{-1} for two nights of Case 1, higher than 0.05 and 0.11 µg m^{-3} hr^{-1} for two nights of Case 2. The mass increase rates of organic nitrate were also significantly higher during two nights of Case 1 (0.13 and 0.19 µg m^{-3} hr^{-1}) than those during the nights of Case 2 (0.04 and 0.06 µg m^{-3} hr^{-1}). The difference of particle growth and mass increase rates between Case 1 and Case 2 could be associated with the concentrations of VOC

615 precursors and/or nighttime oxidants (O$_3$ and NO$_3$ radicals). Note that the mass concentrations of organic nitrate show strong correlations with C$_{10}$H$_{15}$O$_7$N and C$_{15}$H$_{23}$O$_7$N especially during nighttime (Fig. 10), indicating that organic nitrates were formed from the oxidation of monoterpenes and sesquiterpenes by NO$_3$ radicals. This is in line with our previous study that highly functionalized organic nitrates can contribute to nighttime particle growth and OA mass

620 observed at the same area in summer 2016 and 2018 (Huang et al., 2019). In this study, higher concentrations of terpenes were observed during nighttime of both cases. In contrast, during non-particle growth events during nighttime, low concentrations of terpenes, SV-OOA1 were observed generally (Fig. S17). Besides high concentrations of terpenes, the decrease rate of O$_3$ was stronger during the nighttime particle growth periods in Case 1 (-4.6 and -5.0 ppb hr^{-1}) than

625 in Case 2 (-2.1 and -2.9 ppb hr^{-1}). The results suggest the importance of atmospheric oxidants (O$_3$ and NO$_3$ radicals) for nighttime SOA and organic nitrate formation and thus particle growth.

The formation of O_3 and NO_3 radicals are tightly associated with NO_x, thus the reduction of NO_x and O_3 would be helpful to lower the nighttime biogenic SOA formation including potentially toxicologically relevant organic nitrates (Lei et al., 2023) for improving regional air quality.

4 Conclusions

In this study, the composition, sources and evolution processes of VOCs and OA were concurrently investigated by the combination of online mass spectrometry and PMF analysis in a rural forested area in southwest Germany in summer. OA measured by the AMS is the most abundant particulate component, contributing to $67\% \pm 11\%$ of total $PM_{2.5}$ mass. Semi-volatile OA measured by the CHARON-PTR-MS accounted for $62\% \pm 18\%$ of AMS-measured OA. The PMF analysis of VOCs revealed that OVOCs including biogenic-OVOCs, aromatic-OVOCs and aged-OVOCs totally contributed to $77\% \pm 20\%$ of total VOC mixing ratios. AMS-measured OA particle mass was mainly contributed by the oxygenated organic compounds including SV-OOA1, SV-OOA2, LV-OOA and MOOA according to the PMF analysis. Please note, that the relatively large contribution of the marine factor (MOOA) with $22\% \pm 16\%$ is not unexpected in central Europe since we detected substantial contributions of sea salt aerosol in a previous study at a location 2 km west (Shen et al., 2019). Three SOA factors including an aromatic-SOA, a daytime-biogenic SOA, a nighttime-biogenic SOA determined from the CHARON-PMF analysis, totally accounted for $50\% \pm 20\%$ of total CHARON-measured OA mass. We conclude substantial contributions of oxygenated organic compounds in both gas and particle phase. Meanwhile, we illustrated that the oxidation of biogenic terpenes formed more-oxidized VOCs and LV-OOA during daytime, while produced less oxidized VOCs and SV-OOA during nighttime. Combined with air mass back-trajectory analysis, we found that urban air masses significantly enhanced the anthropogenic contributions to OVOCs, and SOA related to aromatic hydrocarbon oxidation. Additionally, particle growth events were frequently observed at this area during early nighttime, similar to recently reported observations in other European forest areas in summer (Kammer et al., 2018; Debevec et al., 2018). We revealed that nighttime particle growth was mainly attributed by the rapid mass increase of semi-volatile organic compounds and organic nitrates from the oxidation of monoterpenes and sesquiterpenes. This study elucidates the relative importance of biogenic and anthropogenic emissions by the combination of PMF analysis of VOCs and OA mass spectral data as well as meteorological conditions. In future, the comparison between the PMF analysis of CHARON-

660   PTR-MS and concurrent FIGAERO-CIMS measurement should be done to provide the detailed oxidation pathways of VOCs leading to SOA formation.

Data availability

Data related to this paper will be available at KIT open data (link will be added).

665

Supplement.

The supplement related to this paper is available.

Author contributions

670   JS and HS designed the measurement campaign. JS, FJ, HZ and LG, HS performed the experimental work. JS did the AMS and PTR-MS data analysis. FJ did the CIMS and aethalometer data analysis. HS and HZ processed the trace gas and meteorological data, respectively. TL gave general comments for this paper. JS wrote the paper with contributions from all the co-authors.

675

Competing interests

At least one of the (co-)authors is a member of the editorial board of Atmospheric Chemistry and Physics

680 **Acknowledgements**

Technical support by the staff at IMK-AAF, and financial support by China Scholarship Council (CSC) for JS, FJ and LG, is gratefully acknowledged. Financial support for the CHARON-PTR-MS by the Modular Observation Solutions for Earth Systems (MOSES) project, a novel observing system of the Helmholtz Association, is gratefully acknowledged.

References

Atkinson, R.: Atmospheric chemistry of VOCs and NOx, Atmospheric Environment, 34, 2063-2101, https://doi.org/10.1016/S1352-2310(99)00460-4, 2000.

Burnett, R. T., Pope, C. A., Ezzati, M., Olives, C., Lim, S. S., Mehta, S., Shin, H. H., Singh, G., Hubbell, B., Brauer, M., Anderson, H. R., Smith, K. R., Balmes, J. R., Bruce, N. G., Kan, H., Laden, F., Prüss-Ustün, A., Turner, M. C., Gapstur, S. M., Diver, W. R., and Cohen, A.: An Integrated Risk Function for Estimating the Global Burden of Disease Attributable to Ambient Fine Particulate Matter Exposure, Environmental Health Perspectives, 122, 397-403, doi:10.1289/ehp.1307049, 2014.

Canagaratna, M. R., Jayne, J. T., Ghertner, D. A., Herndon, S., Shi, Q., Jimenez, J. L., Silva, P. J., Williams, P., Lanni, T., Drewnick, F., Demerjian, K. L., Kolb, C. E., and Worsnop, D. R.: Chase Studies of Particulate Emissions from in-use New York City Vehicles, Aerosol. Sci. Tech., 38, 555-573, 10.1080/02786820490465504, 2004.

Canagaratna, M. R., Jimenez, J. L., Kroll, J. H., Chen, Q., Kessler, S. H., Massoli, P., Hildebrandt Ruiz, L., Fortner, E., Williams, L. R., Wilson, K. R., Surratt, J. D., Donahue, N. M., Jayne, J. T., and Worsnop, D. R.: Elemental ratio measurements of organic compounds using aerosol mass spectrometry: characterization, improved calibration, and implications, Atmos. Chem. Phys., 15, 253-272, 10.5194/acp-15-253-2015, 2015.

Canonaco, F., Slowik, J. G., Baltensperger, U., and Prevot, A. S. H.: Seasonal differences in oxygenated organic aerosol composition: implications for emissions sources and factor analysis, Atmos. Chem. Phys., 15, 6993-7002, 2015.

Chen, G., Canonaco, F., Tobler, A., Aas, W., Alastuey, A., Allan, J., Atabakhsh, S., Aurela, M., Baltensperger, U., Bougiatioti, A., De Brito, J. F., Ceburnis, D., Chazeau, B., Chebaicheb, H., Daellenbach, K. R., Ehn, M., El Haddad, I., Eleftheriadis, K., Favez, O., Flentje, H., Font, A., Fossum, K., Freney, E., Gini, M., Green, D. C., Heikkinen, L., Herrmann, H., Kalogridis, A.-C., Keernik, H., Lhotka, R., Lin, C., Lunder, C., Maasikmets, M., Manousakas, M. I., Marchand, N., Marin, C., Marmureanu, L., Mihalopoulos, N., Močnik, G., Nęcki, J., O'Dowd, C., Ovadnevaite, J., Peter, T., Petit, J.-E., Pikridas, M., Matthew Platt, S., Pokorná, P., Poulain, L., Priestman, M., Riffault, V., Rinaldi, M., Różański, K., Schwarz, J., Sciare, J., Simon, L., Skiba, A., Slowik, J. G., Sosedova, Y., Stavroulas, I., Styszko, K., Teinemaa, E., Timonen, H., Tremper, A., Vasilescu, J., Via, M., Vodička, P., Wiedensohler, A., Zografou, O., Cruz Minguillón, M., and Prévôt, A. S. H.: European aerosol phenomenology − 8: Harmonised source apportionment of organic aerosol using 22 Year-long ACSM/AMS datasets, Environment International, 166, 107325, https://doi.org/10.1016/j.envint.2022.107325, 2022.

Chen, Y., Takeuchi, M., Nah, T., Xu, L., Canagaratna, M. R., Stark, H., Baumann, K., Canonaco, F., Prévôt, A. S. H., Huey, L. G., Weber, R. J., and Ng, N. L.: Chemical characterization of secondary organic aerosol at a rural site in the southeastern US: insights from simultaneous high-resolution time-of-flight aerosol mass spectrometer (HR-ToF-AMS) and FIGAERO chemical ionization mass spectrometer (CIMS) measurements, Atmos. Chem. Phys., 20, 8421-8440, 10.5194/acp-20-8421-2020, 2020.

Crippa, M., El Haddad, I., Slowik, J. G., DeCarlo, P. F., Mohr, C., Heringa, M. F., Chirico, R., Marchand, N., Sciare, J., Baltensperger, U., and Prevot, A. S. H.: Identification of marine and continental aerosol sources in Paris using high resolution aerosol mass spectrometry, J Geophys Res-Atmos, 118, 1950-1963, 10.1002/jgrd.50151, 2013a.

Crippa, M., Canonaco, F., Slowik, J. G., El Haddad, I., DeCarlo, P. F., Mohr, C., Heringa, M. F., Chirico, R., Marchand, N., Temime-Roussel, B., Abidi, E., Poulain, L., Wiedensohler, A., Baltensperger, U., and Prévôt, A. S. H.: Primary and secondary organic aerosol origin by combined gas-particle phase source apportionment, Atmos. Chem. Phys., 13, 8411-8426, 10.5194/acp-13-8411-2013, 2013b.

Crippa, M., Canonaco, F., Lanz, V. A., Äijälä, M., Allan, J. D., Carbone, S., Capes, G., Ceburnis, D., Dall'Osto, M., Day, D. A., DeCarlo, P. F., Ehn, M., Eriksson, A., Freney, E., Hildebrandt Ruiz, L., Hillamo, R., Jimenez, J. L., Junninen, H., Kiendler-Scharr, A., Kortelainen, A. M., Kulmala, M., Laaksonen, A., Mensah, A. A., Mohr, C., Nemitz, E., O'Dowd, C., Ovadnevaite, J., Pandis, S. N., Petäjä, T., Poulain, L., Saarikoski, S., Sellegri, K., Swietlicki, E., Tiitta, P., Worsnop, D. R., Baltensperger, U., and Prévôt, A. S. H.: Organic aerosol components derived from 25 AMS data

740   sets across Europe using a consistent ME-2 based source apportionment approach, Atmos. Chem. Phys., 14, 6159-6176, 10.5194/acp-14-6159-2014, 2014.

Debevec, C., Sauvage, S., Gros, V., Sellegri, K., Sciare, J., Pikridas, M., Stavroulas, I., Leonardis, T., Gaudion, V., Depelchin, L., Fronval, I., Sarda-Esteve, R., Baisnée, D., Bonsang, B., Savvides, C., Vrekoussis, M., and Locoge, N.: Driving parameters of biogenic volatile organic compounds and consequences on new particle formation observed at an eastern Mediterranean background site,
745   Atmos. Chem. Phys., 18, 14297-14325, 10.5194/acp-18-14297-2018, 2018.

DeCarlo, P. F., Kimmel, J. R., Trimborn, A., Northway, M. J., Jayne, J. T., Aiken, A. C., Gonin, M., Fuhrer, K., Horvath, T., Docherty, K. S., Worsnop, D. R., and Jimenez, J. L.: Field-deployable, high-resolution, time-of-flight aerosol mass spectrometer, Analytical Chemistry, 78, 8281-8289, 10.1021/ac061249n, 2006.

750   DeWitt, H. L., Hellebust, S., Temime-Roussel, B., Ravier, S., Polo, L., Jacob, V., Buisson, C., Charron, A., André, M., Pasquier, A., Besombes, J. L., Jaffrezo, J. L., Wortham, H., and Marchand, N.: Near-highway aerosol and gas-phase measurements in a high-diesel environment, Atmos. Chem. Phys., 15, 4373-4387, 10.5194/acp-15-4373-2015, 2015.

Eerdekens, G., Yassaa, N., Sinha, V., Aalto, P. P., Aufmhoff, H., Arnold, F., Fiedler, V., Kulmala, M.,
755   and Williams, J.: VOC measurements within a boreal forest during spring 2005: on the occurrence of elevated monoterpene concentrations during night time intense particle concentration events, Atmos. Chem. Phys., 9, 8331-8350, 10.5194/acp-9-8331-2009, 2009.

Ehn, M., Thornton, J. A., Kleist, E., Sipilä, M., Junninen, H., Pullinen, I., Springer, M., Rubach, F., Tillmann, R., Lee, B., Lopez-Hilfiker, F., Andres, S., Acir, I.-H., Rissanen, M., Jokinen, T.,
760   Schobesberger, S., Kangasluoma, J., Kontkanen, J., Nieminen, T., Kurtén, T., Nielsen, L. B., Jørgensen, S., Kjaergaard, H. G., Canagaratna, M., Maso, M. D., Berndt, T., Petäjä, T., Wahner, A., Kerminen, V.-M., Kulmala, M., Worsnop, D. R., Wildt, J., and Mentel, T. F.: A large source of low-volatility secondary organic aerosol, Nature, 506, 476-479, 10.1038/nature13032, 2014.

Eichler, P., Muller, M., D'Anna, B., and Wisthaler, A.: A novel inlet system for online chemical analysis
765   of semi-volatile submicron particulate matter, Atmos. Meas. Tech., 8, 1353-1360, 10.5194/amt-8-1353-2015, 2015.

Faxon, C., Hammes, J., Le Breton, M., Pathak, R. K., and Hallquist, M.: Characterization of organic nitrate constituents of secondary organic aerosol (SOA) from nitrate-radical-initiated oxidation of limonene using high-resolution chemical ionization mass spectrometry, Atmos. Chem. Phys., 18,
770   5467-5481, 10.5194/acp-18-5467-2018, 2018.

Gao, L., Song, J., Mohr, C., Huang, W., Vallon, M., Jiang, F., Leisner, T., and Saathoff, H.: Kinetics, SOA yields, and chemical composition of secondary organic aerosol from β-caryophyllene ozonolysis with and without nitrogen oxides between 213 and 313 K, Atmos. Chem. Phys., 22, 6001-6020, 10.5194/acp-22-6001-2022, 2022.

775   Gkatzelis, G. I., Coggon, M. M., McDonald, B. C., Peischl, J., Gilman, J. B., Aikin, K. C., Robinson, M. A., Canonaco, F., Prevot, A. S. H., Trainer, M., and Warneke, C.: Observations Confirm that Volatile Chemical Products Are a Major Source of Petrochemical Emissions in U.S. Cities, Environ. Sci. Technol., 55, 4332-4343, 10.1021/acs.est.0c05471, 2021.

Gkatzelis, G. I., Tillmann, R., Hohaus, T., Müller, M., Eichler, P., Xu, K. M., Schlag, P., Schmitt, S. H.,
780   Wegener, R., Kaminski, M., Holzinger, R., Wisthaler, A., and Kiendler-Scharr, A.: Comparison of three aerosol chemical characterization techniques utilizing PTR-ToF-MS: a study on freshly formed and aged biogenic SOA, Atmos. Meas. Tech., 11, 1481-1500, 10.5194/amt-11-1481-2018, 2018a.

Gkatzelis, G. I., Hohaus, T., Tillmann, R., Gensch, I., Müller, M., Eichler, P., Xu, K. M., Schlag, P.,
785   Schmitt, S. H., Yu, Z., Wegener, R., Kaminski, M., Holzinger, R., Wisthaler, A., and Kiendler-Scharr, A.: Gas-to-particle partitioning of major biogenic oxidation products: a study on freshly formed and aged biogenic SOA, Atmos. Chem. Phys., 18, 12969-12989, 10.5194/acp-18-12969-2018, 2018b.

Hallquist, M., Wenger, J. C., Baltensperger, U., Rudich, Y., Simpson, D., Claeys, M., Dommen, J.,
790   Donahue, N. M., George, C., Goldstein, A. H., Hamilton, J. F., Herrmann, H., Hoffmann, T., Iinuma, Y., Jang, M., Jenkin, M. E., Jimenez, J. L., Kiendler-Scharr, A., Maenhaut, W., McFiggans, G., Mentel, T. F., Monod, A., Prevot, A. S. H., Seinfeld, J. H., Surratt, J. D., Szmigielski, R., and Wildt,

J.: The formation, properties and impact of secondary organic aerosol: current and emerging issues, Atmos. Chem. Phys., 9, 5155-5236, DOI 10.5194/acp-9-5155-2009, 2009.

795 Hellén, H., Praplan, A. P., Tykkä, T., Ylivinkka, I., Vakkari, V., Bäck, J., Petäjä, T., Kulmala, M., and Hakola, H.: Long-term measurements of volatile organic compounds highlight the importance of sesquiterpenes for the atmospheric chemistry of a boreal forest, Atmos. Chem. Phys., 18, 13839-13863, 10.5194/acp-18-13839-2018, 2018.

Hersbach, H., Bell, B., Berrisford, P., Hirahara, S., Horányi, A., Muñoz-Sabater, J., Nicolas, J., Peubey,
800 C., Radu, R., Schepers, D., Simmons, A., Soci, C., Abdalla, S., Abellan, X., Balsamo, G., Bechtold, P., Biavati, G., Bidlot, J., Bonavita, M., De Chiara, G., Dahlgren, P., Dee, D., Diamantakis, M., Dragani, R., Flemming, J., Forbes, R., Fuentes, M., Geer, A., Haimberger, L., Healy, S., Hogan, R. J., Hólm, E., Janisková, M., Keeley, S., Laloyaux, P., Lopez, P., Lupu, C., Radnoti, G., de Rosnay, P., Rozum, I., Vamborg, F., Villaume, S., and Thépaut, J.-N.: The ERA5 global reanalysis, Quarterly
805 Journal of the Royal Meteorological Society, 146, 1999-2049, https://doi.org/10.1002/qj.3803, 2020.

Hodzic, A., Kasibhatla, P. S., Jo, D. S., Cappa, C. D., Jimenez, J. L., Madronich, S., and Park, R. J.: Rethinking the global secondary organic aerosol (SOA) budget: stronger production, faster removal, shorter lifetime, Atmos. Chem. Phys., 16, 7917-7941, 10.5194/acp-16-7917-2016, 2016.

810 Huang, S., Wu, Z., Poulain, L., van Pinxteren, M., Merkel, M., Assmann, D., Herrmann, H., and Wiedensohler, A.: Source apportionment of the organic aerosol over the Atlantic Ocean from 53° N to 53° S: significant contributions from marine emissions and long-range transport, Atmos. Chem. Phys., 18, 18043-18062, 10.5194/acp-18-18043-2018, 2018.

Huang, W., Saathoff, H., Shen, X., Ramisetty, R., Leisner, T., and Mohr, C.: Chemical Characterization
815 of Highly Functionalized Organonitrates Contributing to Night-Time Organic Aerosol Mass Loadings and Particle Growth, Environ. Sci. Technol., 53, 1165-1174, 10.1021/acs.est.8b05826, 2019.

IPCC: Climate Change 2021: The Physical Science Basis. Contribution of Working Group I to the Sixth Assessment Report of the Intergovernmental Panel on Climate Change, Cambridge University
820 Press, Cambridge, United Kingdom and New York, NY, USA, 10.1017/9781009157896, 2021.

Jiang, J., Aksoyoglu, S., El-Haddad, I., Ciarelli, G., Denier van der Gon, H. A. C., Canonaco, F., Gilardoni, S., Paglione, M., Minguillón, M. C., Favez, O., Zhang, Y., Marchand, N., Hao, L., Virtanen, A., Florou, K., O'Dowd, C., Ovadnevaite, J., Baltensperger, U., and Prévôt, A. S. H.: Sources of organic aerosols in Europe: a modeling study using CAMx with modified volatility basis
825 set scheme, Atmos. Chem. Phys., 19, 15247-15270, 10.5194/acp-19-15247-2019, 2019.

Jimenez, J. L., Canagaratna, M. R., Donahue, N. M., Prevot, A. S. H., Zhang, Q., Kroll, J. H., DeCarlo, P. F., Allan, J. D., Coe, H., Ng, N. L., Aiken, A. C., Docherty, K. S., Ulbrich, I. M., Grieshop, A. P., Robinson, A. L., Duplissy, J., Smith, J. D., Wilson, K. R., Lanz, V. A., Hueglin, C., Sun, Y. L., Tian, J., Laaksonen, A., Raatikainen, T., Rautiainen, J., Vaattovaara, P., Ehn, M., Kulmala, M.,
830 Tomlinson, J. M., Collins, D. R., Cubison, M. J., Dunlea, E. J., Huffman, J. A., Onasch, T. B., Alfarra, M. R., Williams, P. I., Bower, K., Kondo, Y., Schneider, J., Drewnick, F., Borrmann, S., Weimer, S., Demerjian, K., Salcedo, D., Cottrell, L., Griffin, R., Takami, A., Miyoshi, T., Hatakeyama, S., Shimono, A., Sun, J. Y., Zhang, Y. M., Dzepina, K., Kimmel, J. R., Sueper, D., Jayne, J. T., Herndon, S. C., Trimborn, A. M., Williams, L. R., Wood, E. C., Middlebrook, A. M.,
835 Kolb, C. E., Baltensperger, U., and Worsnop, D. R.: Evolution of Organic Aerosols in the Atmosphere, Science, 326, 1525-1529, 2009.

Jordan, A., Haidacher, S., Hanel, G., Hartungen, E., Märk, L., Seehauser, H., Schottkowsky, R., Sulzer, P., and Märk, T. D.: A high resolution and high sensitivity proton-transfer-reaction time-of-flight mass spectrometer (PTR-TOF-MS), International Journal of Mass Spectrometry, 286, 122-128,
840 https://doi.org/10.1016/j.ijms.2009.07.005, 2009.

Kammer, J., Perraudin, E., Flaud, P. M., Lamaud, E., Bonnefond, J. M., and Villenave, E.: Observation of nighttime new particle formation over the French Landes forest, Sci. Total Environ., 621, 1084-1092, https://doi.org/10.1016/j.scitotenv.2017.10.118, 2018.

Kari, E., Miettinen, P., Yli-Pirilä, P., Virtanen, A., and Faiola, C. L.: PTR-ToF-MS product ion
845 distributions and humidity-dependence of biogenic volatile organic compounds, International Journal of Mass Spectrometry, 430, 87-97, https://doi.org/10.1016/j.ijms.2018.05.003, 2018.

Kerminen, V.-M., Chen, X., Vakkari, V., Petäjä, T., Kulmala, M., and Bianchi, F.: Atmospheric new particle formation and growth: review of field observations, Environmental Research Letters, 13, 103003, 10.1088/1748-9326/aadf3c, 2018.

850   Kim, S., Karl, T., Helmig, D., Daly, R., Rasmussen, R., and Guenther, A.: Measurement of atmospheric sesquiterpenes by proton transfer reaction-mass spectrometry (PTR-MS), Atmos. Meas. Tech., 2, 99-112, 10.5194/amt-2-99-2009, 2009.

Kirkby, J., Duplissy, J., Sengupta, K., Frege, C., Gordon, H., Williamson, C., Heinritzi, M., Simon, M., Yan, C., Almeida, J., Tröstl, J., Nieminen, T., Ortega, I. K., Wagner, R., Adamov, A., Amorim, A.,
855   Bernhammer, A.-K., Bianchi, F., Breitenlechner, M., Brilke, S., Chen, X., Craven, J., Dias, A., Ehrhart, S., Flagan, R. C., Franchin, A., Fuchs, C., Guida, R., Hakala, J., Hoyle, C. R., Jokinen, T., Junninen, H., Kangasluoma, J., Kim, J., Krapf, M., Kürten, A., Laaksonen, A., Lehtipalo, K., Makhmutov, V., Mathot, S., Molteni, U., Onnela, A., Peräkylä, O., Piel, F., Petäjä, T., Praplan, A. P., Pringle, K., Rap, A., Richards, N. A. D., Riipinen, I., Rissanen, M. P., Rondo, L., Sarnela, N.,
860   Schobesberger, S., Scott, C. E., Seinfeld, J. H., Sipilä, M., Steiner, G., Stozhkov, Y., Stratmann, F., Tomé, A., Virtanen, A., Vogel, A. L., Wagner, A. C., Wagner, P. E., Weingartner, E., Wimmer, D., Winkler, P. M., Ye, P., Zhang, X., Hansel, A., Dommen, J., Donahue, N. M., Worsnop, D. R., Baltensperger, U., Kulmala, M., Carslaw, K. S., and Curtius, J.: Ion-induced nucleation of pure biogenic particles, Nature, 533, 521-526, 10.1038/nature17953, 2016.

865   Leglise, J., Müller, M., Piel, F., Otto, T., and Wisthaler, A.: Bulk Organic Aerosol Analysis by Proton-Transfer-Reaction Mass Spectrometry: An Improved Methodology for the Determination of Total Organic Mass, O:C and H:C Elemental Ratios, and the Average Molecular Formula, Analytical Chemistry, 91, 12619-12624, 10.1021/acs.analchem.9b02949, 2019.

Lei, R., Wei, Z., Chen, M., Meng, H., Wu, Y., and Ge, X.: Aging Effects on the Toxicity Alteration of
870   Different Types of Organic Aerosols: A Review, Current Pollution Reports, 10.1007/s40726-023-00272-9, 2023.

Li, H., Canagaratna, M. R., Riva, M., Rantala, P., Zhang, Y., Thomas, S., Heikkinen, L., Flaud, P. M., Villenave, E., Perraudin, E., Worsnop, D., Kulmala, M., Ehn, M., and Bianchi, F.: Atmospheric organic vapors in two European pine forests measured by a Vocus PTR-TOF: insights into
875   monoterpene and sesquiterpene oxidation processes, Atmos. Chem. Phys., 21, 4123-4147, 10.5194/acp-21-4123-2021, 2021.

Li, X. B., Yuan, B., Wang, S., Wang, C., Lan, J., Liu, Z., Song, Y., He, X., Huangfu, Y., Pei, C., Cheng, P., Yang, S., Qi, J., Wu, C., Huang, S., You, Y., Chang, M., Zheng, H., Yang, W., Wang, X., and Shao, M.: Variations and sources of volatile organic compounds (VOCs) in urban region: insights
880   from measurements on a tall tower, Atmos. Chem. Phys., 22, 10567-10587, 10.5194/acp-22-10567-2022, 2022.

Middlebrook, A. M., Bahreini, R., Jimenez, J. L., and Canagaratna, M. R.: Evaluation of Composition-Dependent Collection Efficiencies for the Aerodyne Aerosol Mass Spectrometer using Field Data, Aerosol. Sci. Tech., 46, 258-271, 10.1080/02786826.2011.620041, 2012.

885   Mohr, C., DeCarlo, P. F., Heringa, M. F., Chirico, R., Slowik, J. G., Richter, R., Reche, C., Alastuey, A., Querol, X., Seco, R., Peñuelas, J., Jiménez, J. L., Crippa, M., Zimmermann, R., Baltensperger, U., and Prévôt, A. S. H.: Identification and quantification of organic aerosol from cooking and other sources in Barcelona using aerosol mass spectrometer data, Atmos. Chem. Phys., 12, 1649-1665, 10.5194/acp-12-1649-2012, 2012.

890   Muller, M., Eicher, P., D'Anna, B., Tan, W., and Wisthaler, A.: Direct Sampling and Analysis of Atmospheric Particulate Organic Matter by Proton-Transfer-Reaction Mass Spectrometry, Analytical Chemistry, 89, 10889-10897, 10.1021/acs.analchem.7b02582, 2017.

Müller, M., Mikoviny, T., Jud, W., D'Anna, B., and Wisthaler, A.: A new software tool for the analysis of high resolution PTR-TOF mass spectra, Chemometrics and Intelligent Laboratory Systems, 127,
895   158-165, https://doi.org/10.1016/j.chemolab.2013.06.011, 2013.

Ng, N. L., Canagaratna, M. R., Zhang, Q., Jimenez, J. L., Tian, J., Ulbrich, I. M., Kroll, J. H., Docherty, K. S., Chhabra, P. S., Bahreini, R., Murphy, S. M., Seinfeld, J. H., Hildebrandt, L., Donahue, N. M., DeCarlo, P. F., Lanz, V. A., Prevot, A. S. H., Dinar, E., Rudich, Y., and Worsnop, D. R.: Organic aerosol components observed in Northern Hemispheric datasets from Aerosol Mass Spectrometry,
900   Atmos. Chem. Phys., 10, 4625-4641, 10.5194/acp-10-4625-2010, 2010.

Paatero, P. and Tapper, U.: Positive Matrix Factorization - a Nonnegative Factor Model with Optimal Utilization of Error-Estimates of Data Values, Environmetrics, 5, 111-126, 1994.

Paatero, P., Eberly, S., Brown, S. G., and Norris, G. A.: Methods for estimating uncertainty in factor analytic solutions, Atmos. Meas. Tech., 7, 781-797, 10.5194/amt-7-781-2014, 2014.

905 Pallavi, Sinha, B., and Sinha, V.: Source apportionment of volatile organic compounds in the northwest Indo-Gangetic Plain using a positive matrix factorization model, Atmos. Chem. Phys., 19, 15467-15482, 10.5194/acp-19-15467-2019, 2019.

Peng, Y., Wang, H., Gao, Y., Jing, S., Zhu, S., Huang, D., Hao, P., Lou, S., Cheng, T., Huang, C., and Zhang, X.: Real-time measurement of phase partitioning of organic compounds using a proton-transfer-reaction time-of-flight mass spectrometer coupled to a CHARON inlet, Atmos. Meas. Tech., 16, 15-28, 10.5194/amt-16-15-2023, 2023.

Petit, J. E., Favez, O., Albinet, A., and Canonaco, F.: A user-friendly tool for comprehensive evaluation of the geographical origins of atmospheric pollution: Wind and trajectory analyses, Environ. Modell. Softw., 88, 183-187, 10.1016/j.envsoft.2016.11.022, 2017.

915 Piel, F., Müller, M., Winkler, K., Skytte af Sätra, J., and Wisthaler, A.: Introducing the extended volatility range proton-transfer-reaction mass spectrometer (EVR PTR-MS), Atmos. Meas. Tech., 14, 1355-1363, 10.5194/amt-14-1355-2021, 2021.

Pugliese, G., Piel, F., Trefz, P., Sulzer, P., Schubert, J. K., and Miekisch, W.: Effects of modular ion-funnel technology onto analysis of breath VOCs by means of real-time mass spectrometry, Anal. Bioanal. Chem., 412, 7131-7140, 10.1007/s00216-020-02846-8, 2020.

920 Reyes-Villegas, E., Bannan, T., Le Breton, M., Mehra, A., Priestley, M., Percival, C., Coe, H., and Allan, J. D.: Online Chemical Characterization of Food-Cooking Organic Aerosols: Implications for Source Apportionment, Environ. Sci. Technol., 52, 5308-5318, 10.1021/acs.est.7b06278, 2018.

Seinfeld, J. H. and Pandis, S. N.: Atmospheric chemistry and physics : from air pollution to climate change, 2016.

925 Shen, X. L., Vogel, H., Vogel, B., Huang, W., Mohr, C., Ramisetty, R., Leisner, T., Prevot, A. S. H., and Saathoff, H.: Composition and origin of PM2.5 aerosol particles in the upper Rhine valley in summer, Atmos. Chem. Phys., 19, 13189-13208, 10.5194/acp-19-13189-2019, 2019.

Shrivastava, M., Cappa, C. D., Fan, J., Goldstein, A. H., Guenther, A. B., Jimenez, J. L., Kuang, C., 930 Laskin, A., Martin, S. T., Ng, N. L., Petaja, T., Pierce, J. R., Rasch, P. J., Roldin, P., Seinfeld, J. H., Shilling, J., Smith, J. N., Thornton, J. A., Volkamer, R., Wang, J., Worsnop, D. R., Zaveri, R. A., Zelenyuk, A., and Zhang, Q.: Recent advances in understanding secondary organic aerosol: Implications for global climate forcing, Reviews of Geophysics, 55, 509-559, https://doi.org/10.1002/2016RG000540, 2017.

935 Song, J., Saathoff, H., Gao, L., Gebhardt, R., Jiang, F., Vallon, M., Bauer, J., Norra, S., and Leisner, T.: Variations of PM2.5 sources in the context of meteorology and seasonality at an urban street canyon in Southwest Germany, Atmos. Environ., 119147, https://doi.org/10.1016/j.atmosenv.2022.119147, 2022.

Stein, A. F., Draxler, R. R., Rolph, G. D., Stunder, B. J. B., Cohen, M. D., and Ngan, F.: Noaa's Hysplit 940 Atmospheric Transport and Dispersion Modeling System, B Am Meteorol Soc, 96, 2059-2077, 10.1175/Bams-D-14-00110.1, 2015.

Tani, A., Hayward, S., and Hewitt, C. N.: Measurement of monoterpenes and related compounds by proton transfer reaction-mass spectrometry (PTR-MS), International Journal of Mass Spectrometry, 223-224, 561-578, https://doi.org/10.1016/S1387-3806(02)00880-1, 2003.

945 Ulbrich, I. M., Canagaratna, M. R., Zhang, Q., Worsnop, D. R., and Jimenez, J. L.: Interpretation of organic components from Positive Matrix Factorization of aerosol mass spectrometric data, Atmos. Chem. Phys., 9, 2891-2918, 2009.

Wang, L., Slowik, J. G., Tong, Y., Duan, J., Gu, Y., Rai, P., Qi, L., Stefenelli, G., Baltensperger, U., Huang, R.-J., Cao, J., and Prévôt, A. S. H.: Characteristics of wintertime VOCs in urban Beijing: 950 Composition and source apportionment, Atmospheric Environment: X, 9, 100100, https://doi.org/10.1016/j.aeaoa.2020.100100, 2021.

Wang, L., Slowik, J. G., Tripathi, N., Bhattu, D., Rai, P., Kumar, V., Vats, P., Satish, R., Baltensperger, U., Ganguly, D., Rastogi, N., Sahu, L. K., Tripathi, S. N., and Prévôt, A. S. H.: Source characterization of volatile organic compounds measured by proton-transfer-reaction time-of-flight

mass spectrometers in Delhi, India, Atmos. Chem. Phys., 20, 9753-9770, 10.5194/acp-20-9753-2020, 2020a.

Wang, Y., Mehra, A., Krechmer, J. E., Yang, G., Hu, X., Lu, Y., Lambe, A., Canagaratna, M., Chen, J., Worsnop, D., Coe, H., and Wang, L.: Oxygenated products formed from OH-initiated reactions of trimethylbenzene: autoxidation and accretion, Atmos. Chem. Phys., 20, 9563-9579, 10.5194/acp-20-9563-2020, 2020b.

Wennberg, P. O., Bates, K. H., Crounse, J. D., Dodson, L. G., McVay, R. C., Mertens, L. A., Nguyen, T. B., Praske, E., Schwantes, R. H., Smarte, M. D., St Clair, J. M., Teng, A. P., Zhang, X., and Seinfeld, J. H.: Gas-Phase Reactions of Isoprene and Its Major Oxidation Products, Chem Rev, 118, 3337-3390, 10.1021/acs.chemrev.7b00439, 2018.

Williams, L. R., Gonzalez, L. A., Peck, J., Trimborn, D., McInnis, J., Farrar, M. R., Moore, K. D., Jayne, J. T., Robinson, W. A., Lewis, D. K., Onasch, T. B., Canagaratna, M. R., Trimborn, A., Timko, M. T., Magoon, G., Deng, R., Tang, D., Blanco, E. D. L. R., Prevot, A. S. H., Smith, K. A., and Worsnop, D. R.: Characterization of an aerodynamic lens for transmitting particles greater than 1 micrometer in diameter into the Aerodyne aerosol mass spectrometer, Atmos. Meas. Tech., 6, 3271-3280, 2013.

Wu, C., Bell, D. M., Graham, E. L., Haslett, S., Riipinen, I., Baltensperger, U., Bertrand, A., Giannoukos, S., Schoonbaert, J., El Haddad, I., Prevot, A. S. H., Huang, W., and Mohr, C.: Photolytically induced changes in composition and volatility of biogenic secondary organic aerosol from nitrate radical oxidation during night-to-day transition, Atmos. Chem. Phys., 21, 14907-14925, 10.5194/acp-21-14907-2021, 2021.

Wu, Y., Liu, D., Tian, P., Sheng, J., Liu, Q., Li, R., Hu, K., Jiang, X., Li, S., Bi, K., Zhao, D., Huang, M., Ding, D., and Wang, J.: Tracing the Formation of Secondary Aerosols Influenced by Solar Radiation and Relative Humidity in Suburban Environment, J. Geophys. Res.-Atmos., 127, e2022JD036913, https://doi.org/10.1029/2022JD036913, 2022.

Xu, L., Suresh, S., Guo, H., Weber, R. J., and Ng, N. L.: Aerosol characterization over the southeastern United States using high-resolution aerosol mass spectrometry: spatial and seasonal variation of aerosol composition and sources with a focus on organic nitrates, Atmos. Chem. Phys., 15, 7307-7336, 10.5194/acp-15-7307-2015, 2015.

Yuan, B., Shao, M., de Gouw, J., Parrish, D. D., Lu, S., Wang, M., Zeng, L., Zhang, Q., Song, Y., Zhang, J., and Hu, M.: Volatile organic compounds (VOCs) in urban air: How chemistry affects the interpretation of positive matrix factorization (PMF) analysis, Journal of Geophysical Research: Atmospheres, 117, https://doi.org/10.1029/2012JD018236, 2012.

Zaytsev, A., Koss, A. R., Breitenlechner, M., Krechmer, J. E., Nihill, K. J., Lim, C. Y., Rowe, J. C., Cox, J. L., Moss, J., Roscioli, J. R., Canagaratna, M. R., Worsnop, D. R., Kroll, J. H., and Keutsch, F. N.: Mechanistic study of the formation of ring-retaining and ring-opening products from the oxidation of aromatic compounds under urban atmospheric conditions, Atmos. Chem. Phys., 19, 15117-15129, 10.5194/acp-19-15117-2019, 2019.

Zhang, Q., Jimenez, J. L., Canagaratna, M. R., Ulbrich, I. M., Ng, N. L., Worsnop, D. R., and Sun, Y. L.: Understanding atmospheric organic aerosols via factor analysis of aerosol mass spectrometry: a review, Anal. Bioanal. Chem., 401, 3045-3067, 2011.

Zhou, W., Xu, W., Kim, H., Zhang, Q., Fu, P., Worsnop, D. R., and Sun, Y.: A review of aerosol chemistry in Asia: insights from aerosol mass spectrometer measurements, Environ. Sci. Process Impacts, 22, 1616-1653, 10.1039/D0EM00212G, 2020.

1005
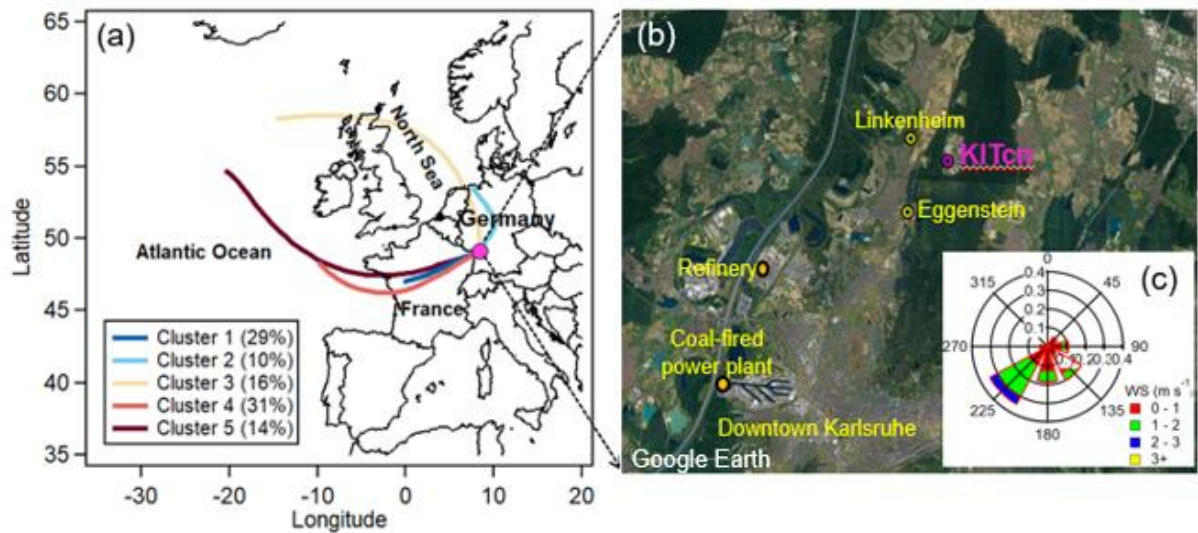
1010 **Figure 1.** Location of the measurement site along with the clusters of air mass back-trajectories. (a) five major air mass clusters, (b) map of sampling location (KITcn), Eggenstein (LUBW air quality monitor station), two industrial sources (a refinery and a coal-fired power plant) and Linkenheim (a sampling site in summer 2016, Huang et al., 2019) (©Google Earth). (c) Wind rose plot for the entire campaign.

1015
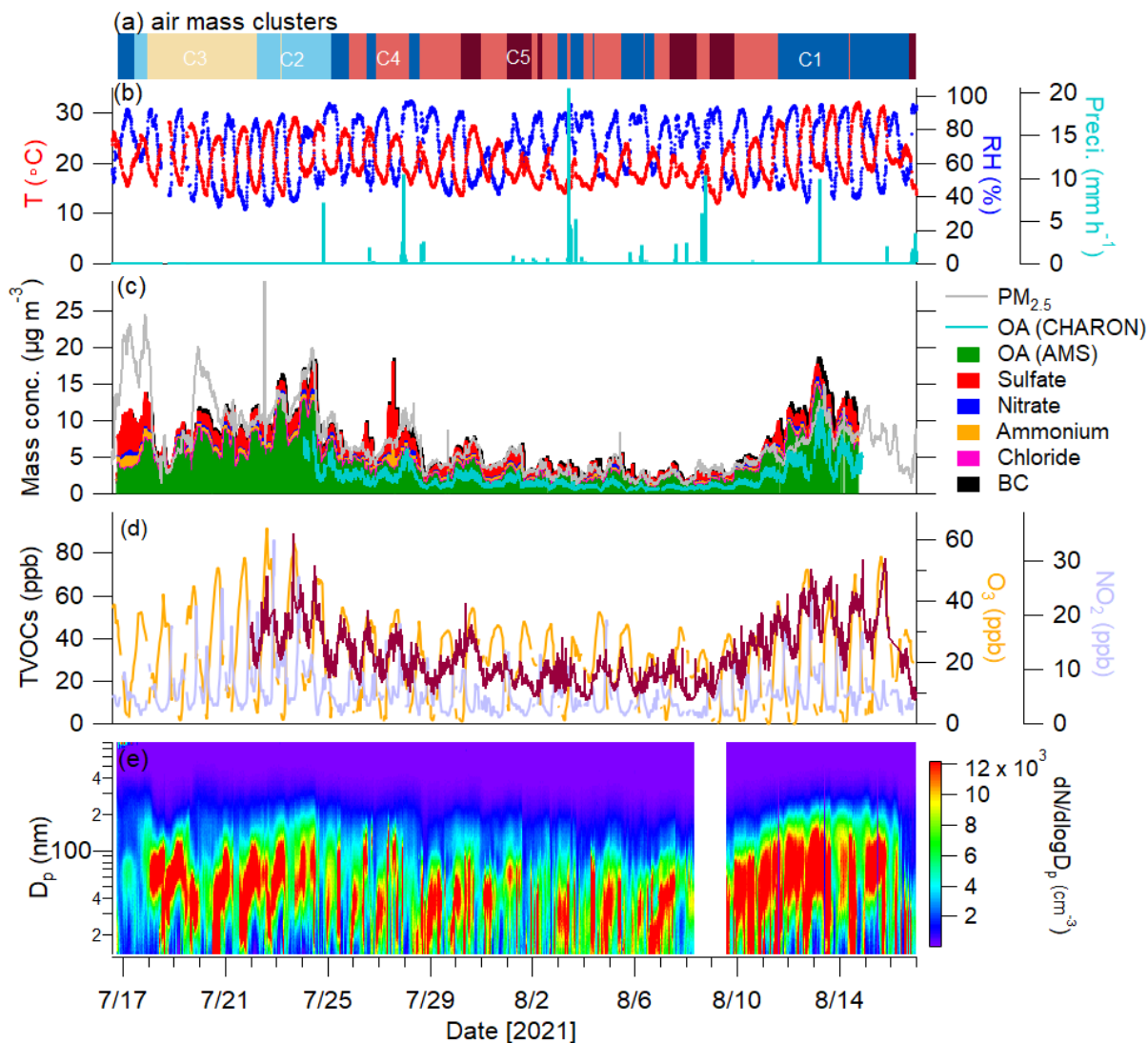
Figure 2. Time series of (a) origins of air mass clusters; (b) temperature (T) and relative humidity (RH) and precipitation; (c) mass concentrations of PM2.5 measured by the OPC, OA measured by the CHARON, OA, sulfate, nitrate, ammonium, chloride measured by the AMS and BC; (d) concentrations of total VOCs (TVOCs, brown line), O_3 and NO_2; (e) particle number size distribution measured by the SMPS.
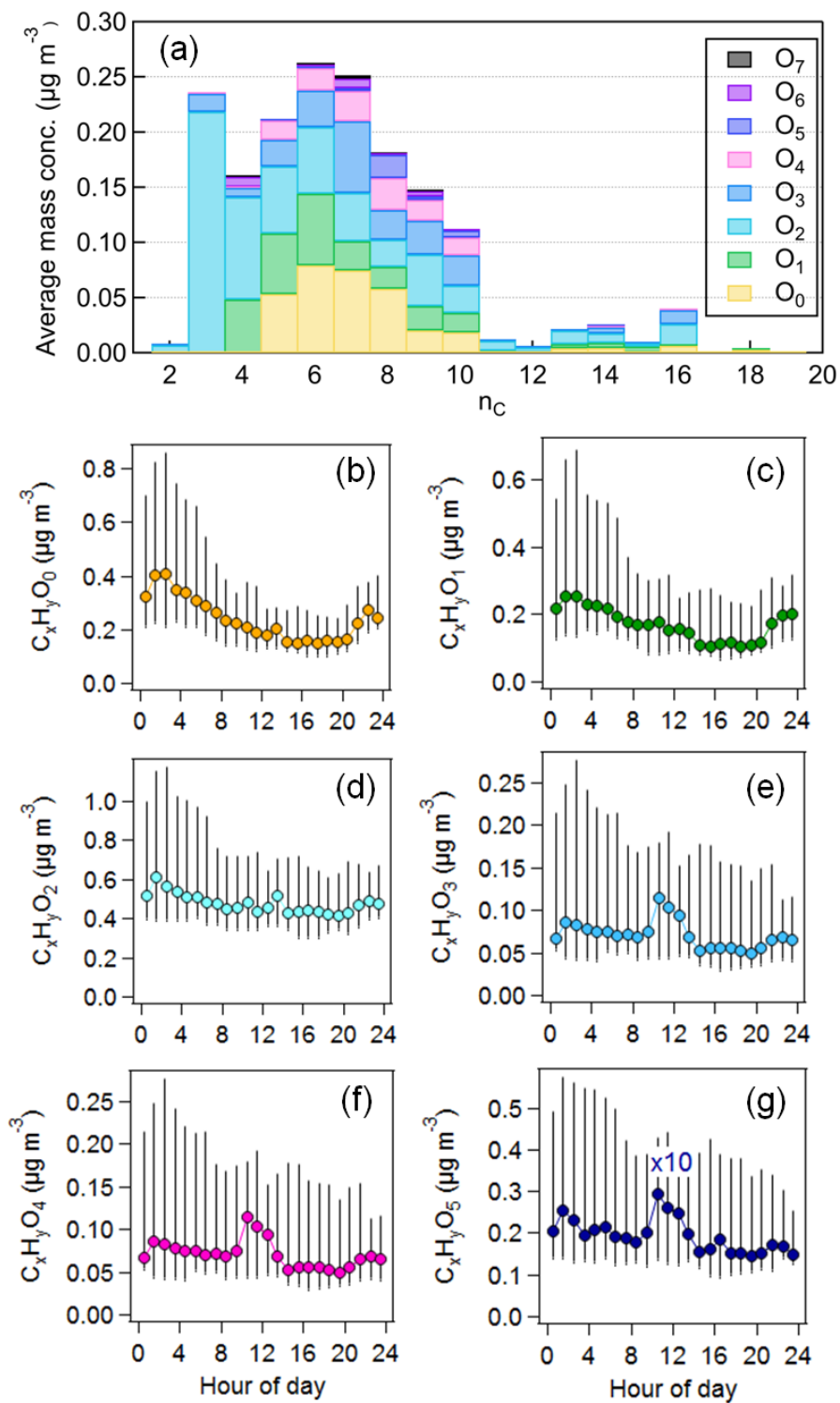
Figure 3. (a) Average mass distributions of identified particulate organic species ($C_xH_yO_z$) resolved by the carbon and oxygen numbers (n_C and n_O) from the CHARON-PTR-MS; (b-g) Average diurnal variations of $C_xH_yO_{0-5}$. The sticks represent the 25th and 75th percentiles.
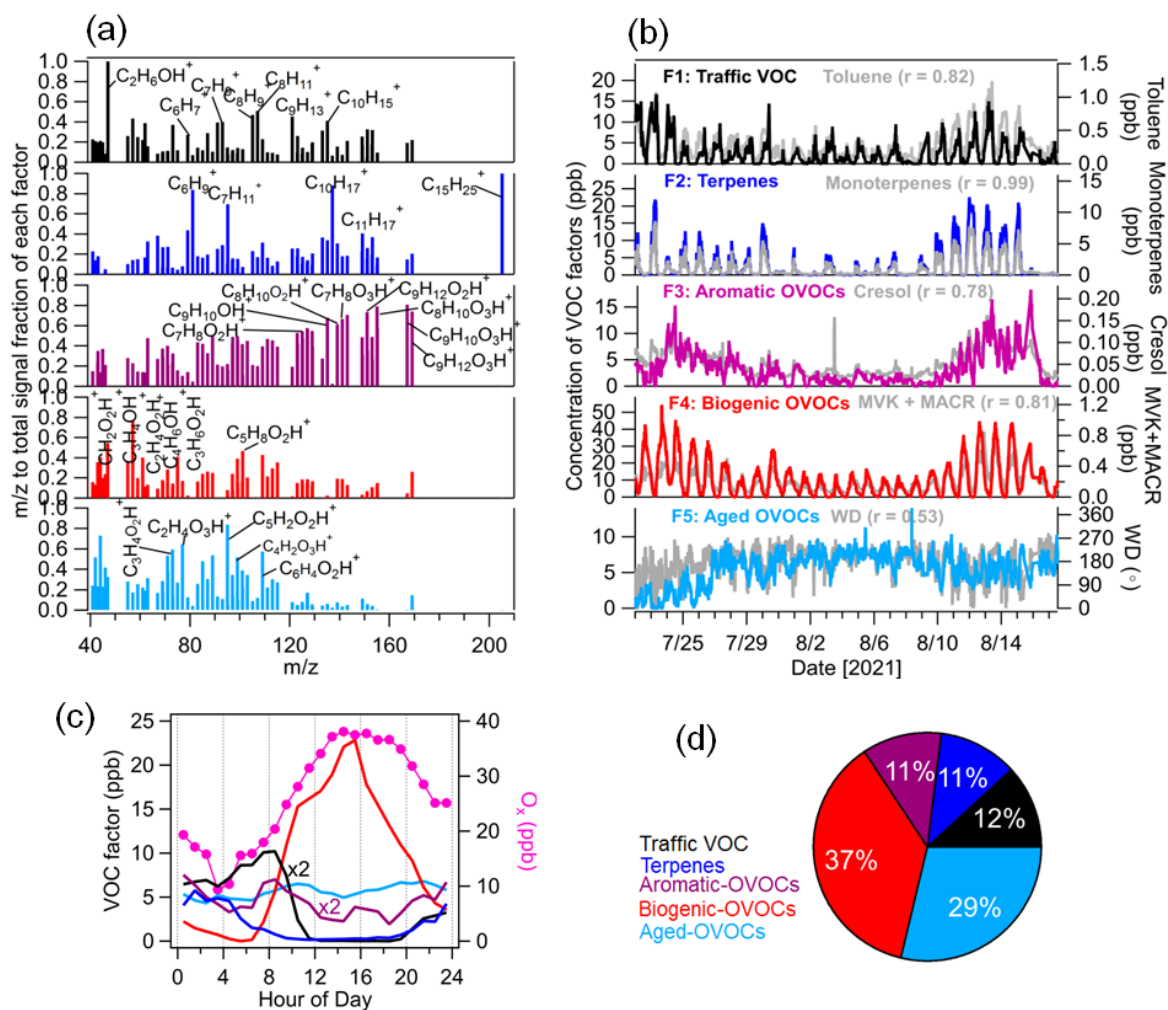
Figure 4. Source apportionment of VOCs measured by the PTR-MS. (a) Normalized VOC factor spectra from PMF analysis on the *m/z* peaks (relative contribution of each factor to each ion); (b) time series of VOC factors including traffic, terpenes, aromatic-OVOCs, biogenic-OVOCs and aged-OVOCs with external tracer species including toluene, monoterpenes, cresol, MVK + MACR and wind direction (WD); (c) median diurnal variations of VOC factors and O_x ($NO_2 + O_3$); (d) relative contribution of each VOC factors to total VOC concentrations.
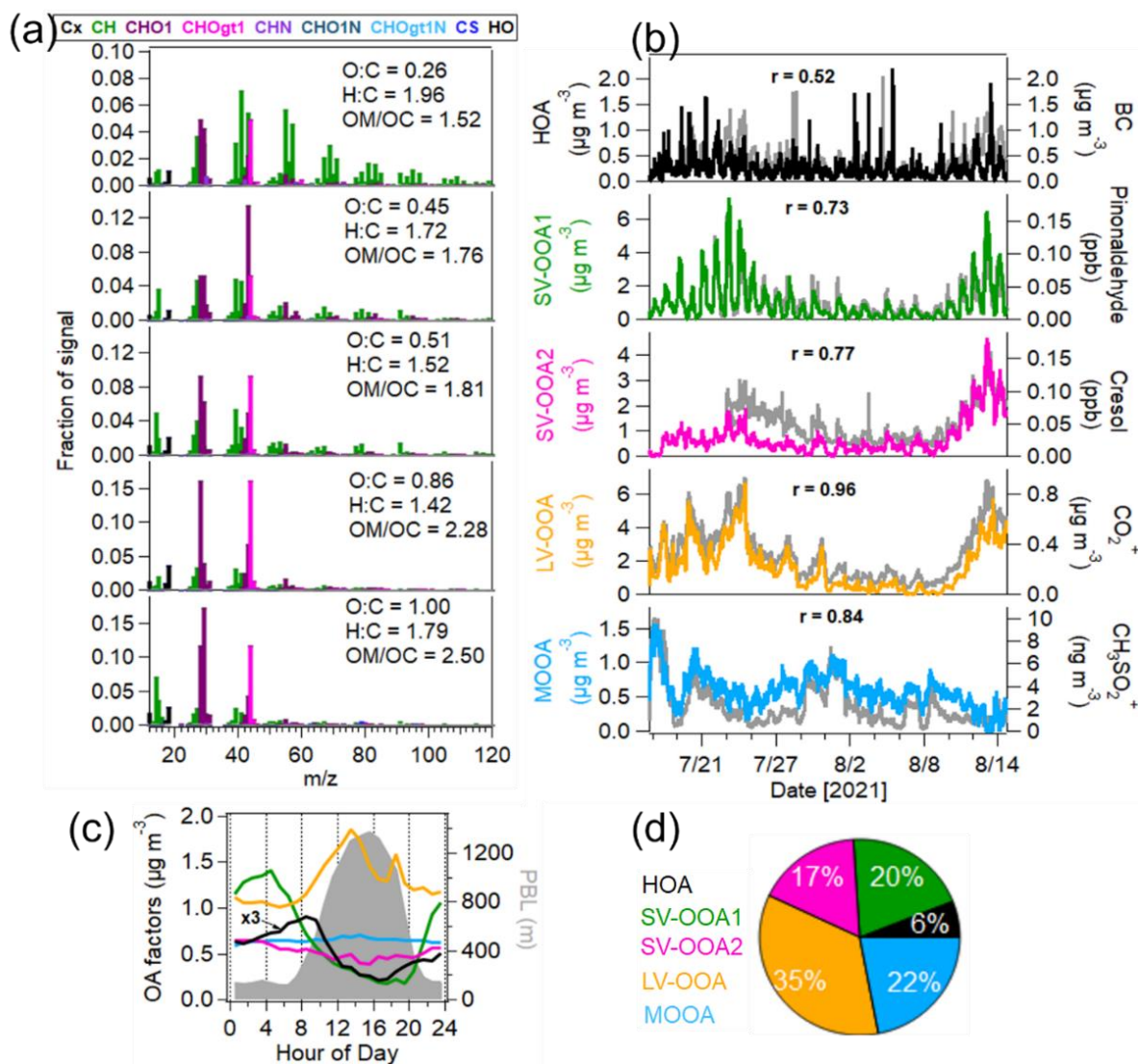
Figure 5. Source apportionment of OA measured by the AMS. (a) Mass spectra of OA factors: hydrocarbon-like OA (HOA), two semi-volatile oxygenated OA (SV-OOA1 and SV-OOA2), low-volatility oxygenated OA (LV-OOA) and marine oxygenated OA (MOOA); (b) time series of OA factors and external tracer species (BC, pinonaldehyde and cresol measured by the PTR-MS, CO_2^+ and $CH_3SO_2^+$ measured by the AMS); (c) median diurnal variations of OA factors and PBL height; and (d) mass fraction of OA factors in total OA mass.
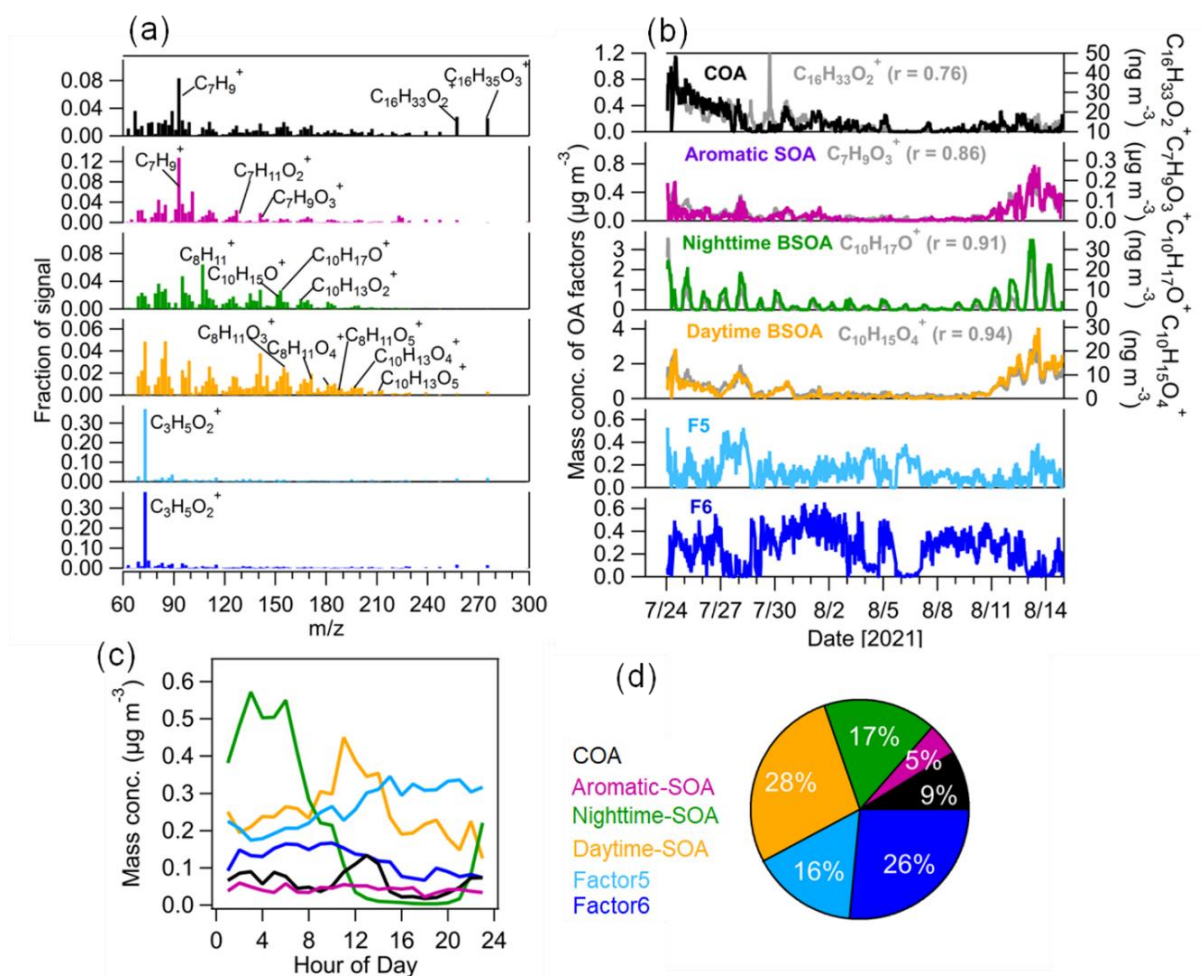
Figure 6. Source apportionment of OA measured by the CHARON-PTR-MS. (a) mass spectra of six factors of OA from PMF analysis; (b) time series of six OA factors including cooking-related OA (COA), aromatic hydrocarbon oxidation-related SOA (aromatic-SOA), nighttime and daytime biogenic SOA (Daytime-SOA and nighttime-SOA) with marker ions including $C_{16}H_{33}O_2^+$, $C_7H_9O_3^+$, $C_{10}H_{17}O^+$ and $C_{10}H_{15}O_4^+$, respectively. Two factors (F5 and F6) dominated by $C_3H_5O_2^+$ could not be assigned to specific sources; (c) median diurnal variations of OA factors; (d) relative contributions of each OA factor to total OA mass.
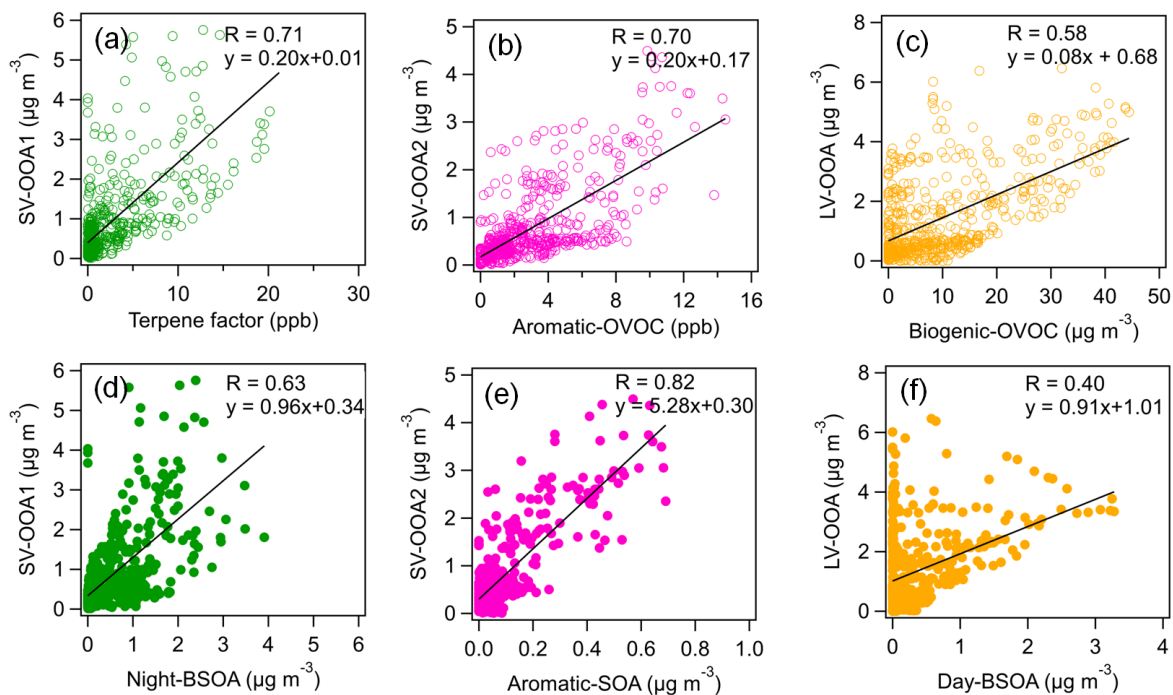
1050

Figure 7. Correlations of three AMS-measured SOA factors (SV-OOA1, SV-OOA2, LV-OOA) with VOC factors (terpene factor, aromatic-OVOC, biogenic-OVOC) and CHARON-measured SOA factors (nighttime-BSOA, aromatic-SOA, daytime-BSOA).
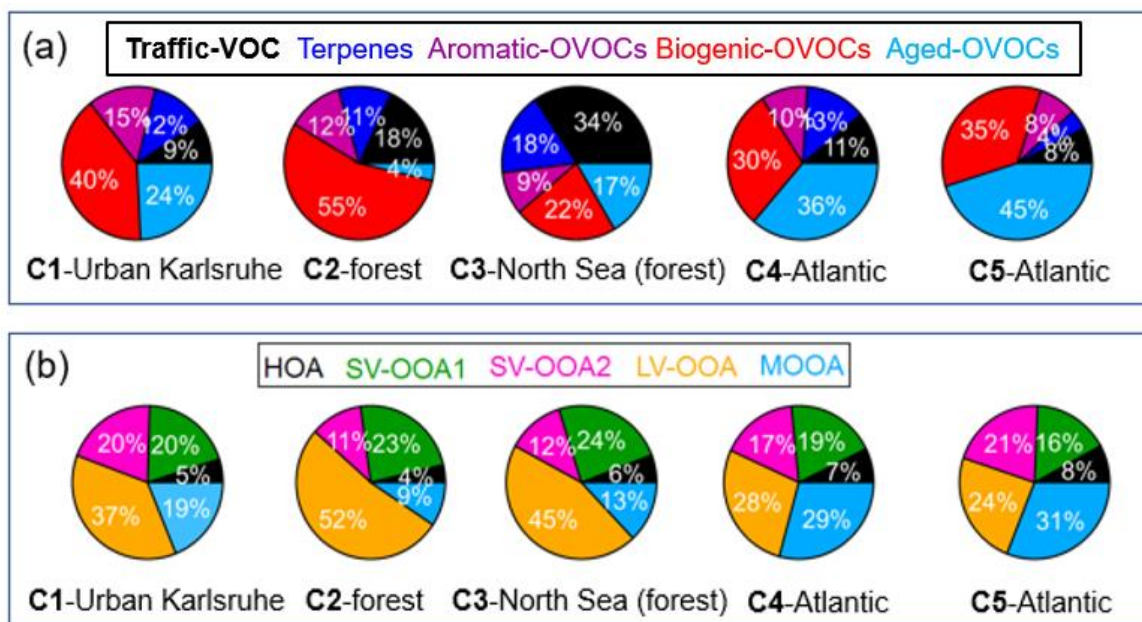
1055

Figure 8. Relative contributions of (a) VOC factors to total VOC mixing ratios and (b) OA factors to AMS-measured OA mass for five different air mass clusters (C1-Urban Karlsruhe, C2-forest, C3-North Sea (forest), C4-Atlantic, C5-Atlantic).
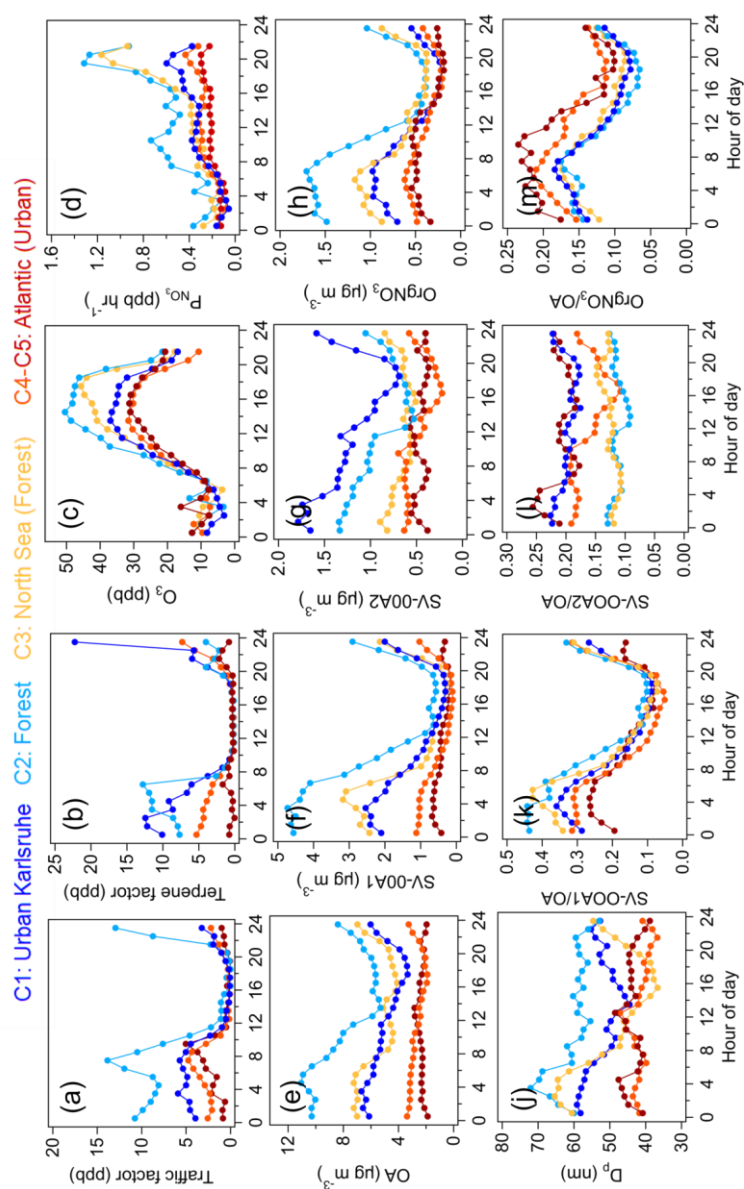
Figure 9. Diurnal variations of VOC precursors, oxidants, SOA factors and particle size for different air mass clusters: (a-b) traffic VOC and terpene factors measured by the PTR-MS; (c) O_3 mixing ratios; (d) production rate of NO_3 radicals; (e-h) mass concentrations of OA, SV-OOA1, SV-OOA2 and organic nitrate (OrgNO$_3$) measured by the AMS; (j) geometric mean particle size (D$_p$); (k-m) mass fractions of SV-OOA1, SV-OOA2 and OrgNO$_3$ in total OA mass.
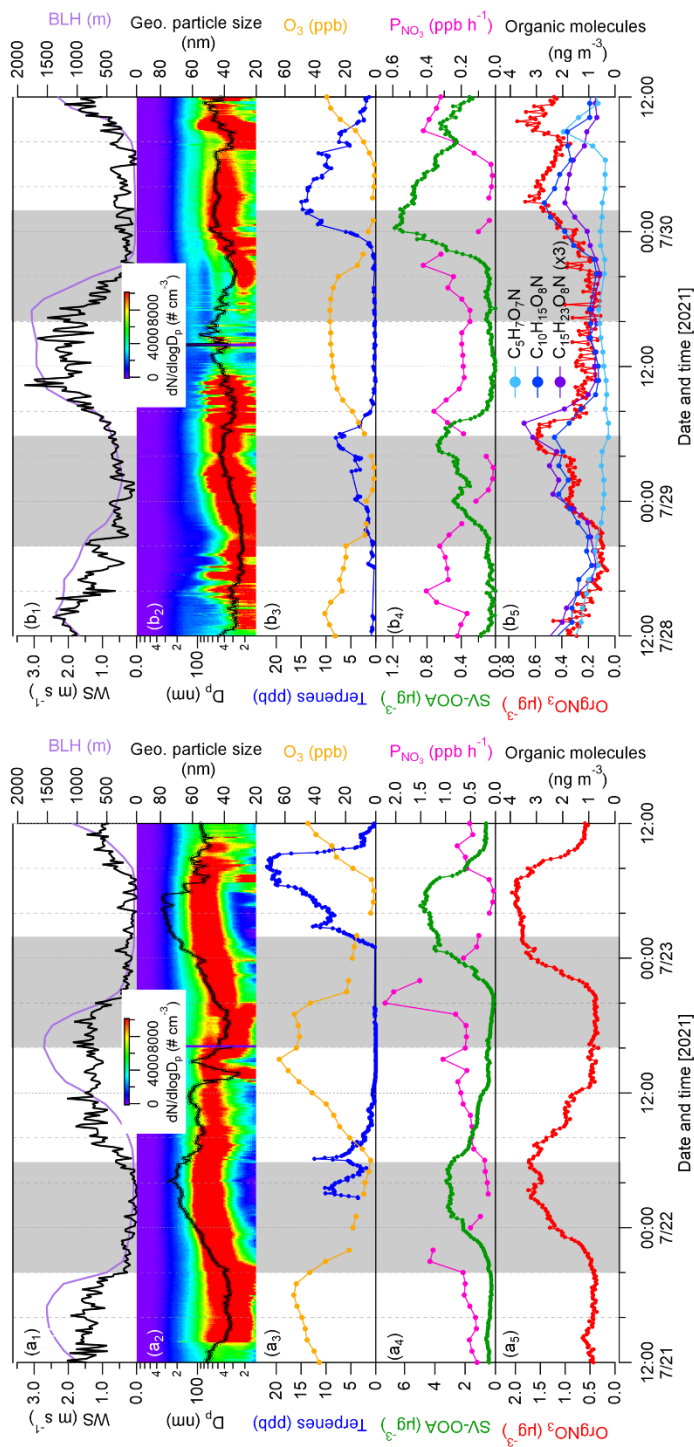
Figure 10. Cases showing the nighttime particle growth events as marked in gray shaded areas. Time series of wind speed, boundary layer height, particle number size distributions and geometric mean particle size, and mixing ratios of terpenes factor and O_3, production rate of nitrate radicals (P_{NO_3}), and mass concentrations of SV-OOA1 and organic nitrate calculated from the AMS during 21st-23rd (a1-a5) and 28th-30th July, 2021 (b1-b5). Three particulate organic nitrate molecules ($C_5H_7O_7N$, $C_{10}H_{15}O_8N$, $C_{15}H_{23}O_8N$) detected by the FIGAERO-CIMS are plotted in (b5).